Title
Deciphering the tropomyosin code: Uncovering how different tropomyosin isoforms bind and assemble on actin filaments

Author
Rodriguez, Johnny

Publication Date
2020

Peer reviewed|Thesis/dissertation

Deciphering the tropomyosin code: Uncovering how different tropomyosin isoforms bind and assemble on actin filaments

by
Johnny Rodriguez

DISSERTATION
Submitted in partial satisfaction of the requirements for degree of
DOCTOR OF PHILOSOPHY

in

Biochemistry and Molecular Biology

in the

GRADUATE DIVISION
of the
UNIVERSITY OF CALIFORNIA, SAN FRANCISCO

Approved:

DocuSigned by:
Dyche Mullins
E4FB70A20A7546F...

Dyche Mullins
Chair

DocuSigned by:
Sophie Dumont

Sophie Dumont

DocuSigned by:
Sy Redding
A9C649A156A64AA...

Sy Redding

Committee Members

Acknowledgements and Dedications

An old African proverb once stated, “It takes a village to raise a child”. A PhD is an accomplishment one gets from applying the knowledge and experiences received from countless number of people to solve an underlying problem. Although I will personally acknowledge the people who have made the greatest impact, so many people were instrumental in helping me complete this dissertation. To those not mentioned, thank you from the bottom of my heart.

First of all, I would like to thank my advisor and mentor, Dyche Mullins. Dyche constantly utilizes his engineering background to think deeply about the biophysical mechanisms of the actin cytoskeleton. The hypotheses he envisions are some of the most clever and logical ways to explain the new data. Just by being around Dyche, he gave me the proper tools to think very critically about science and I will always be thankful for that. Dyche is also an amazing human being. Despite going through periods where my experiments just did not work, he remained very supportive and enthusiastic about my project. I always left his office with the energy to make progress on my project.

Next, I would like to thank my rotation mentor, lab mate, and friend Natalie A. Petek-Seoane. Natalie is a very rigorous biochemist and the reason the tropomyosin project became so fruitful the last couple of years. The constant betting and arguing about science made the last year couple of years in the Mullins lab very enjoyable. She is very supportive and always goes out of her way to help out in any way she could.

I would also like to thank Jenny Hsiao and Lauren Goins for allowing me to join the tropomyosin team. They took their time to introduce me to the tropomyosin literature. They also enlightened me on where they thought the project was headed and taught me

the assays I needed to get started.

I want to thank the rest of the Mullins lab for making the lab environment a great place to learn and talk about science. Peter Bieling for occasionally providing some of his vast knowledge in actin biochemistry and microscopy. Samuel Lord for helping me think critically about my project and creating ways to make data analysis less cumbersome. Justin Salat, Terri Lee, Arthur Charles-Orzag, and PJ Buske for making the center bay enjoyable. In addition, special shout out to Terri for helping me develop the habit of setting weekly goals and pushing me to think about life after graduate school.

I would like to thank the rest of my thesis committee, Sophie Dumont, Sy Redding, and former member Ron Vale. They are all extremely talented scientists and it is always an honor to receive advice from them. Although we talked infrequently, our discussions have helped me create a fantastic scientific story for my thesis project.

I would like to thank my UCSF Tetrad classmates for making life outside of work enjoyable. In particular, I would like to thank the members of the Hufflepuff house: Andre Lazar, Fernando Meza Gutierrez, and Joel Hrit. These fine gentlemen were instrumental in helping me transition from SoCal to San Francisco. The gym workouts, our conversations, and just hanging out was something I always looked forward to when I was not in lab.

I would also like to thank my friends Fernando Meza Gutierrez and Karina Perlaza. They are amazing people to be around with and have always included Kelly and I in their social circle. Kelly and I definitely enjoyed living like adults with them.

Lastly, I would like to thank my friends, Justin Salat and Nick Sanchez. Justin and Nick have joined me in in my quest to fish for some rainbow trout and bass. It has been

fun learning to fish with them and will definitely miss these weekend trips. I also enjoyed playing games with them and meeting the countless number of Nick's friends.

In addition, I would like to thank my family:

Primero, quiero agradecer a mi mamá, María de Los Ángeles Flores. Mi mamá es la mujer más trabajadora que conozco. Aunque es madre soltera, siempre se aseguraba de que tuviéramos comida en la mesa y que tuviéramos todo lo necesario para la escuela. Había un tiempo cuando mi hermano, mi hermana, y yo íbamos a tres diferentes escuelas, pero ella siempre encontraba la manera de como llevarnos y recogernos de la escuela. Mi mama es la razón por la que he logrado mis sueños. Por estas razones, le dedico este doctorado, porque sin ella, nunca estaría donde estoy hoy.

Next, I would like to thank my dad, Luis Rodriguez. From a very young age, dad taught me four big lessons: always follow your dreams, never give up, always make time for family, and to always remain faithful to God. These four big lessons have helped define the person that I have become and definitely helped me get through this very difficult yet rewarding part of my life. Thank you, dad.

I would also like to thank my brother Chris and my sister-in-law Marisa. I have watched their relationship and careers blossom into something wonderful. They have broken so many cultural barriers and have become great role models for our family. It is a pleasure having them in my life and always look forward to spending the holidays with them.

I would like to thank my sister Michelle. Michelle has overcome some of the hardest obstacles a person can ever face and will soon be graduating with a bachelor's degree. I am thankful to have her as a sister and always look forward to spending time with her.

Next, I would like to thank my brother Joshua. Joshua is the youngest in the family and has been a pleasure watching him grow up. Although I don't see him often, we have built a strong relationship and I am thankful to have him in my life.

Finally, I would like to thank my fiancé, my best friend, and my soulmate, Kelly Crotty. We started dating in graduate school and she has been by my side through the best and worst of times. As the years go by, our love grows stronger and stronger. Although we have spent the last year apart, the wait is definitely worth it. I look forward to spending the rest of our lives together and will always love you.

Deciphering the tropomyosin code: Uncovering how different tropomyosin isoforms bind and assemble on actin filaments

Johnny Rodriguez

Abstract

Actin is a highly conserved protein that assembles into many three-dimensional structures, each with a unique subset of actin-binding proteins that produces a unique three-dimensional architecture capable of performing a specific function. These actin networks are central to cellular processes such as motility, adhesion, endocytosis, and division. Yet how actin filaments can recruit the correct subset of actin-binding proteins while avoiding the incorrect ones remains unclear. Recent literature demonstrated that in non-muscle cells, a different tropomyosin isoform(s) is present at every single actin network. Tropomyosins are coiled-coil proteins that regulate access to actin filament binding sites and now widely believed to determine which actin structure will be built. Despite this, we know very little about the assembly and function of tropomyosins on actin filaments. This is partly due to the fact that mammalian cells express over 20 different tropomyosin isoforms. In the Mullins lab, we have chosen *Drosophila melanogaster* S2 cells as the model system for the study of tropomyosins because S2 cells are easy to grow, highly susceptible to gene inhibition using RNAi, have well-characterized actin networks, and most importantly, only express three tropomyosin isoforms. In this dissertation, we investigate how these *Drosophila* tropomyosins assemble on actin filaments. In Chapter 1, I designed a microfluidic system that allows us to manipulate microscopy experiments at a level never before achieved in the Mullins lab. In Chapter 2,

I characterize binding and dynamic properties of the classic Drosophila tropomyosin Tm1A. In Chapter 3, I discovered how to get Drosophila tropomyosins Tm1J and Tm2A to bind actin filaments and then characterize these tropomyosins.

Table of Contents

List of Figures

Chapter One

Design and assembly of microfluidic chambers for use in Total Internal Reflection Fluorescence Microscopy

Contributions

Chapter 1 project creation and execution was performed by Johnny Rodriguez. Chapter 1 writing was also done by Johnny Rodriguez. The laser-cut double-sided tape chamber discussed in the chapter was inspired by a talk with Nico Stuurman. The use of 2-way valves was inspired by Sy Redding.

Introduction

Total Internal Reflection Fluorescence (TIRF) Microscopy revolutionized the actin cytoskeleton field by allowing researchers to directly visualize fluorophore-labeled actin filaments. Serendipitously, the actin filament barbed end incorporates unbleached monomers from solution faster than the pointed end, making the barbed end significantly brighter and therefore distinguishable from the pointed end. Visualizing single actin filaments via TIRF microscopy allows for direct measurements of actin dynamics (Amann and Pollard, 2001; Kuhn and Pollard, 2005) and was instrumental in elucidating the mechanisms of actin-binding proteins such as formins (Kovar and Pollard, 2004), VASP (Hansen and Mullins, 2010), and WASP (Bieling et al., 2018).

Performing TIRF experiments with actin filaments does possess technical limitations. First, TIRF imaging has to be performed with methylcellulose, a viscous additive that can promote bundling of actin filaments. The evanescent wave produced from total internal reflection restricts imaging to <200 nm from the coverslip surface (Breitsprecher et al., 2009). When this restriction is coupled to the Brownian motion exhibited by actin filaments, imaging becomes impossible. Methylcellulose helps reduce Brownian motion, allowing the actin filaments to be imaged using TIRF (Uyeda et al., 1990; Kohler et al., 2008). However, methylcellulose can have artificial effects on actin and the actin binding proteins being studied.

Next, the solution of the actin filaments inside the imaging chamber cannot be changed without washing away the actin filaments in the imaging frame of view. To avoid this problem, tethering reagents, such as biotinylated-myosin (Kron and Spudich, 1986) or biotin-phalloidin (Hansen and Mullins, 2010), can be used to immobilize actin filaments

to the coverslip surface, but this results in perturbed filaments that are unable to move/rotate freely and have certain actin binding sites blocked.

Lastly, imaging actin filaments that are able to move stochastically in solution makes data analysis difficult. There have been recent advances in image analysis (Smith et al., 2010; Li et al., 2009), but published scripts and free plugins are usually tailored to perform on specific task. This forces the end user to eventually create a custom code, which is not always trivial.

Microfluidics have recently been applied to single actin filament TIRF, circumventing these technical limitations. Jegou and colleagues tethered actin filaments from one of their ends and applied microfluidic flow to essentially keep the filaments near the coverslip surface (Jegou et al., 2011). This allows the user to limit perturbations to actin filament ends, minimizing potential artifacts. During microfluidic TIRF, actin filaments movement is very minimal, eliminating the need for highly viscous additives and simplifying image analysis.

For my thesis project, I have implemented microfluidic TIRF to visualize the interaction between *Drosophila melanogaster* tropomyosins and *Drosophila melanogaster* non-muscle actin. While building the microfluidic contraption, I discovered two technical limitations: the microfluidic chamber and the tubing assembly. In this chapter, I discuss how I solved these problems.

To perform microfluidics TIRF, Jegou and colleagues needed a microfluidic chamber that allowed biochemical solutions to flow into and out of the chamber (Jegou et al., 2011). Since the flow velocity in a microfluidic chamber is directly proportional to the

cross-sectional area of the chamber, the chamber dimensions need to be built with high precision to eliminate flow variability between experiments.

Jegou and colleagues used photolithography to create a high precision microfluidic chamber on polydimethylsiloxane (PDMS). The resulting PDMS chamber is then plasma bonded via a plasma cleaner to microscope glass coverslips, creating a watertight seal. To prevent proteins from nonspecifically sticking to the coverslip surface or PDMS walls, Bovine Serum Albumin (BSA) or poly-L-Lysine polyethylene glycol (PLL-PEG) is flowed into the chamber, passivating the surface. Unfortunately, tropomyosins and formins are extremely sticky proteins and thus require higher quality passivation than just BSA or PLL-PEG. Silane PEGs provide superior passivation compared to the previously mentioned methods. Unfortunately, these methods require alcohols or organic solvents (Bieling et al., 2010) that I demonstrated are incompatible with PDMS.

Design 1: The vacuum sealed PDMS chamber

One approach is to passivate the glass coverslip before fusing the PDMS to the chamber. However, once the coverslip is passivated, the coverslip cannot be plasma bonded to the PDMS because the plasma cleaner will destroy the passivation on the coverslip surface. Therefore, another method of fusing the PDMS chamber to the glass coverslip surface is required.

Inspired by the Rohit lab (Bose et al., 2013), I invented a PDMS chamber that can be sealed to a coverslip using a vacuum pump. This design circumvents the need for plasma bonding, allowing any desired passivation method to be used on the glass coverslip surface. Since the PDMS chamber is still created using photolithography,

chambers are created at very high precision, eliminating flow variability during experiments. Photolithography also allows the end user to create very intricate flow chambers, including chambers with complex three-dimensional structures (Thian et. al., 2006).

Materials

0.5mm Biopsy Punch (World Precision Instruments, 504528)

2 Table Clamps (Grainger, 190033019)

2-Propanol (Millipore Sigma, I9516-4L)

2mm Biopsy Punch (World Precision Instruments, 504531)

3-inch Silicon Wafer (University Wafers, 447)

6-inch x 6-inch ½ inch Quartz Glass Slabs

Borosilicate Glass Plate 6” x 6” x 3/4” (McMaster-Carr, 8476K16)

Bucket with 2-inch hole drilled into the bottom center

Dremel High Performance Rotary Tool (Dremel, 4000)

G3P Spin Coater (Specialty Coating Systems)

Glass Drying Dish (Pyrex, C31758)

Heavy-Duty Petri Dishes (CELLTREAT, 229638)

High Precision Glass Coverslips (Bioscience Tools, CSHP-No1.5-22x22)

Hot Plate (Corning, 6795-600D)

Mixing Spatulas for use in Drill (Mixtik, 405-5301)

Oven (Analytik Jena US, 95-0030-01)

Polished Quartz Glass Plate 6” x 6” x 1” (Technical Glass)

Precision Knife (Elmer's, XZ3601)

Propylene Glycol Monomethyl Ether Acetate (Millipore Sigma, 484431-4L)

Stir Bar (Bel-Art, F37110-0002)

Stir Plate (Corning, 6796-210)

SU-8 3025 Photoresist (Kayaku Advanced Materials Inc, Y311072 0500L1GL)

SYLGARD 184 Silicone Elastomer Kit (Dow, 2646340)

T-Cube LED Driver (Thor Labs, LEDD1B)

T-Cube Power Supply Unit (Thor Labs, KPS101)

UV Lamp, 120mW, 700mA (Thor Labs, M365L2-C1)

Vacuum Desiccator (Bel-Art, 08-594-16B)

Wafer Handling Tweezers (Techni-Tool, 2WFG)

Methods

Construction of the SU-8 Master for PDMS Chambers

1. Use Autodesk AutoCAD or equivalent computer-aided design software to design the microfluidic chamber that will be printed on a 3-inch photolithography mask. Make sure to put your name on it. This will be used to determine the orientation of the photomask in later steps. Photolithography masks can be ordered from any major lithography company. I used the drawing guidelines found on the following URL:

http://stmichaelshospitalresearch.ca/wp-content/uploads/2019/05/Photomask_Design_Rules.pdf

2. Use the wafer tweezers to handle the wafer.

3. Take the 3-inch silicon wafer and make sure it is free of dust particles. Dust can create defects on the microfluidic patterns, potentially ruining the patterns.

4. Place the silicon wafer in the spin coater and pipette 3 mL of SU-8 photoresist onto the wafer. Close the spin coater lid to prevent the photoresist from splattering.

5. Use the SU-8 photoresist manual to identify the proper protocol needed to obtain desired photoresist thickness. This thickness will determine the height of the chamber so make sure to choose this height carefully. In our case, we needed a thickness of 45 μm and so we did an initial spin at 500 rpm for 5-10 seconds with acceleration of 100 rpm/second. We immediately did a second spin at 2250 rpm for 30 seconds with an acceleration of 300 rpm/second.

6. Place the wafer on a 135°C hot plate, which will heat the actual wafer to 95°C. Heat the wafer for the required time. This time can be obtained in the SU-8 photoresist manual. In our case, the wafer was baked for 15 minutes.

7. Take the soft baked SU-8 wafer and place the wafer on top of a glass slab. Place the photomask on top of the wafer. If the words on the mask are legible, the mask in in the correct orientation. Place a second glass slab on top and clamp the entire sandwich together. This ensures that the photomask is completely contacting the surface of the silicon wafer, maximizing micropattern resolution.

8. Place the bucket over the sandwich. Place the UV lamp on the hole, illuminating only inside of the bucket. Expose the sandwich with the UV lamp at maximum intensity for 2 minutes, 30 seconds.

9. Place the exposed silicon wafer onto the 135°C hot plate. Heat the wafer for the time required. This time can be obtained in the SU-8 photoresist manual. In our case, the wafer is baked for 5 minutes.

10. Prepare a glass tray filled with Propylene Glycol Monomethyl Ether Acetate (PGMEA) and place it on a stir plate. Add a stir bar and set the stir speed to the highest speed without splashing. Place the silicon wafer into the tray and incubate for 8 minutes.

11. Take the wafer and squirt fresh PGMEA on the wafer, removing the dirty PGMEA and any residual SU-8. Dry the wafer with filtered house air.

12. Place the wafer on the 135°C hot plate and bake for 30 minutes.

13. Place the wafer into a petri dish. The SU-8 master is now ready.

14. To prepare the PDMS, mix 10 parts Base with 1 part Catalyst. For a petri dish, we prepare 50 grams Base with 5 grams Catalyst. Attach the plastic spatula to the Dremel Drill and mechanically mix the solution for 30-40 seconds. Degas for 45 minutes to remove air bubbles.

15. Carefully pour the PDMS into the Petri Dish that contains the silicon wafer, making sure to prevent the formation of bubbles. Place the Dish in a 65°C oven and cure the PDMS for 2-4 hours.

16. Once cured, cut out the PDMS mold out by using a precision knife. The SU-8 Master in the Petri Dish can be reused as long as the silicon wafer is not cracked and the micropatterns are still intact.

Assembly of the PDMS vacuum Chamber

1. For this section, prepare 22mm x 22mm coverslips with your favorite passivation method. In our case, we use (3-Glycidyloxypropyl) trimethoxysilane and NH_2-PEG-5000-methoxy to passivate glass (Bieling et al., 2010).

2. Use the 0.5 mm biopsy punch to puncture holes into the chamber inlet and outlet positions on the PDMS slab.

2. Use the 2 mm biopsy punch to puncture a hole for the vacuum chamber.

3. Attach a passivated coverslip to the PDMS chamber. The passivated side of the coverslip should face the micropattern side of the PDMS slab. Insert the vacuum line into the vacuum inlet and turn on the vacuum. The vacuum seals the PDMS to the coverslip.

4. The chamber is now ready for use.

Design 2: The laser-cut, double-sided tape chamber

The vacuum sealed PDMS chamber protocol allows very complex microchannels to be assembled onto a coverslip that is treated with virtually any passivation method. However, since the chamber needs to be sealed with a continuous vacuum, the chamber cannot be transported and therefore requires assembly to take place on the microscope. This prevents the user to assemble microfluidic chambers ahead of time, making it very cumbersome. If the user's microchannels do not require complex structures, the laser-cut, double-sided tape chamber is probably the chamber of choice.

Inspired by Nico Stuurman, this chamber is created by sandwiching laser-cut, double-sided tape with a microscope slide and a coverslip. Although the microchannel

resolution from double-sided, laser-cut tape is not as high as resolution obtained from photolithography, channels with a width of 500 nm and a height of 50 um are attainable. This resolution should be high enough for any microfluidic TIRF experiment that images actin filaments. Like the previous method, this method allows the user to treat the coverslip with any passivation method. In addition, the chambers can be assembled ahead of time and transported, making experimental setup easier than the vacuum-sealed chamber.

Materials

0.75mm Diamond Drill Bit, Collet 1/32 (Kingsley North Inc, 1-0500)

3D-Printed Slide Holder (Template on www.mullinslab.ucsf.edu/protocols)

Double-sided Tape, 50□m thickness (3M, 93005LE)

Dremel High Performance Rotary Tool (Dremel, 4000)

Dremel Keyless Chuck for use with bits with 1/32-inch shanks (Dremel, 4486)

Dremel WorkStation (Dremel, 220-01)

Empty p1000 Pipette Box or 4” x 4” x 4” Acrylic Box

Glass Staining Dish and Slide Rack (Electron Microscopy Sciences, 70312-30)

High Precision Glass Coverslips (Bioscience Tools, CSHP-No1.5-22x22)

Lab Tape (Fisher Scientific, 1590110R)

Laser Cutter (Universal Laser Systems, VLS3.5)

Microscope Plain Glass Slides (Fisher Scientific, 12-544-1)

NanoPort Assembly (IDEX Health & Science, N-333)

Quick Setting Epoxy (ACE, 18613)

Methods

Laser cutting the Double-sided Tape into chambers

1. Use Adobe Illustrator or equivalent vector graphics software to create the desired micropattern. Make sure the curves and lines are RGB = 255, 0, 0 (aka True Red). This color tells the laser cutter to where to cut.

2. Open the micropattern in Adobe Illustrator and select print/VLS3.5 to transfer the file to the laser cutter.

3. Use the paper preset to prepare the laser cutter to cut a sheet of double-sided tape.

4. Optimize the laser power and laser speed to figure the settings that are just strong enough to cut the tape. The laser has day-to-day variability and thus the laser needs to be calibrated every time before use. Be careful not to use too much laser power and too low of a speed, which can melt the tape, ruining the chambers.

5. Once the double-sided tape is cut, the tape is ready for use.

Microscope Slide Preparation

1. Assemble the Dremel drill onto the Dremel workstation, installing the keyless chuck and the diamond drill bit. Place the 3D printed slide holder into the p1000 tip box and fill up the box with water.

2. Using lab tape, lightly tape the edges of a double-sided tape chamber to a microscope slide. This will serve as the template for drilling the inlets and outlets. This double-sided tape can be reused as a template for multiple microscope slides.

3. Place the microscope slide + template onto the slide holder, making sure both the slide and the slide holder are completely submerged in water. Water prevents the drill from locally heating the glass, preventing the glass from shattering.

4. Using the template, drill the inlets and outlets on microscope slide. When finished, remove the template.

5. Repeat steps 2-4 for as many microscope slides are needed.

6. Rack the drilled microscope slides onto the stainless-steel slide rack. Place the rack into a staining dish and fill the dish with 1% Hellmanex in ultrapure water. Incubate the slides for 2 hours.

7. Rinse the slides with copious amounts of ultra-pure water to remove residual Hellmanex.

8. Dry the slides with Nitrogen or Argon gas.

9. Take a NanoPort and apply a thin layer of epoxy to the bottom of the NanoPort, making sure not to glue close the inlet port.

10. Glue a NanoPort on every single inlet and outlet.

11. Let the glue cure at room temperature overnight.

12. The slides are now ready to use.

Double-sided Tape Chamber Assembly

1. For this section, prepare 22mm x 22mm coverslips with your favorite passivation method. In our case, we use (3-Glycidyloxypropyl) trimethoxysilane and NH_2-PEG-5000-methoxy to passivate glass (Bieling et al., 2010).

2. Peel the first protective film of a double-sided tape chamber and attach it to the microscope slide, aligning the drilled holes with the double-sided tape inlets and outlets.

3. Peel the second protective film of the double-sided tape and attach the coverslip, passivated side towards the tape. Use lens paper to press the coverslip into the tape, creating a strong seal.

4. Bake the assembly in a 70°C oven for 5 minutes. This step cures the tape to the glass.

5. The chamber is now ready to use.

Connecting and handling of microfluidic chambers during experiment

When working with microfluidic chambers, one of the biggest obstacles is how to reliably connect and handle the chambers without introducing air bubbles into the system. Air bubbles create problems because they can lead to pressure variations, possibly destroying the experiment being performed. In addition, air bubbles are detrimental to proteins, often leaded to protein unfolding and protein aggregation. After countless hours of experimenting with many connection and handling protocols, I have identified a highly reliable method, inspired by Sy Redding, that involves the use of two-way valves.

Materials

B-Casein (Millipore Sigma, C6905)

Flangeless Ferrule ETFE (Idex Health & Science, P-200)

Flangeless Nuts PEEK (Idex Health & Science, P-235X)

Luer Adapter (Idex Health & Science, P-659)

NanoTight Fittings (Idex Health & Science, F-333N)

Pluoronic Acid F-127 (Millipore Sigma, P2443)

PTFE 1/16” Tubing (ElveFlow, LVF-KTU-15)

Syringe Pump (Harvard Apparatus, Model 22)

Syringe, 1 mL (Fisher Scientific, 14-817-25)

Methods

Connecting the chamber with 1/16 line

1. Set up the 2-way valve by connecting the following lines into the valve ports in clockwise order: sample line, chamber line, no line, waste line. Use the flangeless ferrules and nuts for connections.

2. Connect the 2-way valve chamber line to the chamber. If using chamber design 1, insert line ends into the inlet holes made by the biopsy punch. If using chamber design 2, use NanoTight fittings to screw lines into the chamber inlets.

3. Add an outlet line to every chamber outlet. Use the proper connections as described in step 2.

4. Connect NanoTight fittings to the 2-way valve sample line. Add a Luer Adapter, allowing sample to be added using a Luer syringe.

4. Place 2-way valve waste line end and the chamber waste line end into a waste beaker.

5. Switch the 2-way valve to flow from sample line to waste.

6. Load a syringe with ultrapure water and hook up syringe to sample line via Luer adapter.

7. Inject the water until the lines are completely hydrated and free of bubbles.

8. Switch the 2-way valve to flow from sample line to chamber and inject water using a syringe pump to load sample at 100μL/min. Syringe pump is necessary to avoid bursting of microfluidic chamber.

9. Repeat steps 5-8 with 1% Pluronic Acid in your buffer of choice. This solution is necessary to block the lines, preventing nonspecific absorption of your sample to the tubing.

10. Repeat steps 5-8 with 0.5mg/mL B-casein in your buffer of choice. This solution is necessary to block the lines, preventing nonspecific absorption of your sample to the tubing.

11. Repeat steps 5-8 with buffer to be used for experiment.

12. Chamber is now ready for experiment.

**Note: If dead volume is an issue, Elveflow sells a kit that allows 1/32 tubing to be used with 1/16 fittings (Elveflow product SKU: LVF-KTU-16).

There is always room for improvement

Although the microfluidic assembly is very reliable, I discovered that it still takes two sets of hands to get through an entire experiment. The main reason is that the 2-way valves I described are manually operated. Therefore, chamber preparation and channel switching during experiments need to be manually performed. To overcome this, I

recommend automating the valves, allowing the user to focus their attention on the actual experiment.

The last place for improvement is the selection of double-sided tape for the double-sided tape chamber. Although the tape is strong enough to be used with a syringe pump or pressurized microfluidic system, it cannot handle the force exerted by a hand-operated syringe. This limits the user to a syringe pump, which can add time to chamber preparation. As of 2018, 3M produced only one kind of double-sided tape that was 50 μm in thickness. I propose to eventually upgrade to a stickier tape.

Conclusion

In this chapter, we introduced two different microfluidic chamber designs: the vacuum sealed PDMS chamber and the laser cut, double-sided tape chamber. The main advantage of these novel chamber designs is the ability to use any glass passivation method. For our research, these designs allowed us to use the GOPTS-PEG method, the Mullins lab gold standard for glass passivation.

Even with these chambers, microfluidics can become very cumbersome without a reliable method for connecting and handling microfluidic chambers during an experiment. We therefore developed a method that uses affordable 2-way valves to connect/disconnect, flow solutions, and transport microfluidic chambers without introducing bubbles that would destroy experiments. In summary, these advancements will help researchers more easily apply microfluidics to their single molecule microscopy experiments.

References

Amann, K., Pollard, T. (2001). Direct real-time observation of actin filament branching mediated by Arp2/3 complex using total internal reflection fluorescence microscopy. *Proceedings of the National Academy of Sciences,* 98(26), 15009-15013.

Bieling, P., Telley, I., Hentrich, C., Piehler, J., Surrey, T. (2010). Chapter 28 Fluorescence microscopy assays on chemically functionalized surfaces for quantitative imaging of microtubule, motor, and +TIP dynamics. *Methods in Cell Biology*, 95(), 555-580.

Bieling, P., Hansen, S., Akin, O., Li, T., Hayden, C., Fletcher, D., Mullins, R. (2018). WH2 and proline-rich domains of WASP-family proteins collaborate to accelerate actin filament elongation. *The EMBO Journal*, 37(1), 102-121.

Bose, S., Singh, R., Hanewich-Hollatz, M., Shen, C., Lee, C., Dorfman, D., Karp, J., Karnik, R. (2013). Affinity flow fractionation of cells via transient interactions with asymmetric molecular patterns. *Scientific Reports*, 3(1), 2329.

Breitsprecher, D., Kiesewetter, A., Linkner, J., Faix, J. (2009). Analysis of actin assembly by in vitro TIRF microscopy. *Chemotaxis, Methods and Protocols.* (Clifton, N.J.) 571(), 401-415.

Hansen, S., Mullins, R. (2010). VASP is a processive actin polymerase that requires monomeric actin for barbed end association. *The Journal of Cell Biology*, 191(3), 571-584.

Jégou, A., Niedermayer, T., Orbán, J., Didry, D., Lipowsky, R., Carlier, M., Romet-Lemonne, G. (2011). Individual actin filaments in a microfluidic flow reveal the

mechanism of ATP hydrolysis and give insight into the properties of profilin. *PLoS Biology*, 9(9), e1001161.

Köhler, S., Lieleg, O., Bausch, A. (2008). Rheological characterization of the bundling transition in F-actin Solutions induced by methylcellulose. *PLoS ONE*, 3(7), e2736.

Kovar, D., Pollard, T. (2004). Insertional assembly of actin filament barbed ends in association with formins produces piconewton forces. *Proceedings of the National Academy of Sciences*, 101(41), 14725-14730.

Kuhn, J., Pollard, T. (2005). Real-time measurements of actin filament polymerization by Total Internal Reflection Fluorescence Microscopy. *Biophysical Journa*l, 88(2), 1387-1402.

Kron, S., Spudich, J. (1986). Fluorescent actin filaments move on myosin fixed to a glass surface. *Proceedings of the National Academy of Sciences*, 83(17), 6272-6276.

Li, H., Shen, T., Smith, M., Fujiwara, I., Vavylonis, D., Huang, X. (2009). Automated actin filament segmentation, tracking, and tip elongation measurements based on open active contour models. *Proceedings of the IEEE International Symposium on Biomedical Imaging: From Nano to Macro 2009*, 1302-1305

Smith, M., Li, H., Shen, T., Huang, X., Yusuf, E., Vavylonis, D. (2010). Segmentation and tracking of cytoskeletal filaments using open active contours. *Cytoskeleton*, 67(11), 693-705.

Thian, S., Tang, Y., Fuh, J., Wong, Y., Lu, L., Loh, H. (2006). Micro-rapid-prototyping via multi-layered photo-lithography. *The International Journal of Advanced Manufacturing Technology*, 29(9-10), 1026-1032.

Uyeda, T., Kron, S., Spudich, J. (1990). Myosin step size estimation from slow sliding movement of actin over low densities of heavy meromyosin. *Journal of Molecular Biology*, 214(3), 699-710.

Chapter Two

Characterization of Drosophila tropomyosin Tm1A on Drosophila actin filaments

Contributions

Experiments

Protein constructs and protein purifications were performed by Johnny Rodriguez. Figures 2.1A, 2.1C-F, 2.2-2.3, and 2.7A-D were performed by Johnny Rodriguez. Figures 2.1B and 2.7E-G were performed by Natalie A. Petek-Seoane. The rest of the experiments in this chapter were performed equally by Johnny Rodriguez and Natalie A. Petek-Seoane.

Figure Production

Figure production for figures 2.1, 2.2, and 2,3 were performed by Johnny Rodriguez. Figure production for figures 2.4, 2.5, 2.6, and 2.7 were performed by Natalie A. Petek-Seoane.

Chapter writing

Chapter introduction, discussion, figure captions, and materials and methods were written by Johnny Rodriguez. Results was written by Natalie A. Petek-Seoane as a draft for the pointed-end paper manuscript.

Introduction

Actin is one of the most highly conserved and abundant proteins in non-muscle eukaryotic cells. *In vivo*, actin subunits assemble into filaments, which further assemble into several different actin structures. Each of these actin structures contains a unique subset of actin regulatory proteins, producing a unique three-dimensional architecture with a specialized function. These actin networks are involved in a plethora of cellular processes, including cell morphology (Pollard and Cooper, 2009), plasma membrane protrusion (Svitkina and Borisy, 1999; Iwasa and Mullins, 2007), cell adhesion (Heath and Dunn, 1978; Gumbiner, 1996), and the assembly of a contractile ring during cell division (Mabuchi, 1994; Balasubramanian et al., 2004). The question is: How do non-muscle cells assemble different structures if they all use actin as the main building block? One answer to this question may be provided with tropomyosins.

Tropomyosins are alpha-helical, coiled-coil dimers that polymerize head-to-tail to form continuous cables that wrap around entire actin filaments (Whitby et al., 2000; Ecken et al., 2016; Yamada et al., 2020). By binding all along the actin filaments, tropomyosins can act as the actin gatekeeper: controlling which actin-binding proteins have access to actin filaments and which ones don't. Mammalian non-muscle cells encode for four different tropomyosin genes which, through alternative splicing, give rise to over two dozen different tropomyosin isoforms (Schevzov et al., 2011). Each isoform is sorted to different actin networks (Percival et al., 2000; Dalby-Payne et al., 2003). Since there is a unique tropomyosin isoform at each actin network and tropomyosins have the ability to control access to actin filaments, it is possible that tropomyosins control which actin

structure is assembled. Therefore, unraveling the basic properties of tropomyosins can help reveal how the different cellular actin structures are assembled.

Unfortunately, with the overwhelming number of possible isoforms, determining the function of each isoform has proven to be very complex. We chose *Drosophila melanogaster* S2 cells as the model organism for uncovering the roles of tropomyosins isoforms. The S2 cell line is the quintessential model system because S2 cells are easy to grow, are highly susceptible to gene inhibition using RNAi (Rogers and Rogers, 2008), have well-characterized actin networks (D'Ambrosio and Vale, 2010; Rogers et al., 2003; Iwasa and Mullins, 2007), and express only three tropomyosin isoforms: Tm1A, Tm1J, and Tm2A (Goins and Mullins, 2015). Like mammalian cells, each *Drosophila* tropomyosin has a distinct localization pattern. When any of the tropomyosins are mutated, the cells exhibit morphological or cell division defects, strongly suggesting that each *Drosophila* tropomyosin isoform is required.

To understand the functions of all three tropomyosins, we need to biochemically characterize each tropomyosin. In this chapter, we focus on the biochemical characterization of tropomyosin Tm1A.

Results

Purification and characterization of *Drosophila melanogaster* actin from Schneider 2 (S2) cells

Since our previous observations suggest that unlike other actin-binding proteins, tropomyosin may prefer actin from one species over another, we decided to study *D. melanogaster* tropomyosin Tm1A in the context of its host actin. We therefore purified actin from S2 cells, a macrophage-like cell line derived from the late stage *D. Melanogaster* embryo, using a modified version of the method described by (Rogers and Rogers, 2008) (Figure 2.1A). *Drosophila melanogaster* S2 actin (hereafter called 'S2 actin') polymerizes into two-stranded helical filaments similar in appearance to other known non-muscle actins (Holmes et al., 1990) (Figure 2.1B). Pyrene fluorescence determined that S2 actin polymerizes with similar kinetics to other non-muscle actins (Figure 2.1C). Phalloidin-actin seeded single filaments grew at a rate of 13.7 subunits/second per μM to the end of actin filaments (Figure 2.1D-F).

Binding of tropomyosin isoform Tm1A to S2 Actin

In order to describe the binding properties of Tm1A to S2 actin versus other host actins, we first wanted to characterize Tm1A in the absence of actin. To determine the oligomerization state of Tm1A, we turned to analytical ultracentrifugation (AUC). A sedimentation velocity titration of 1.2 μM Tm1A at various concentrations of KCl resulted in a progressive decrease of the sedimentation coefficient as KCl concentration increased, leveling off between 400mM and 1.1M KCl (Figure 2.2). This is indicative of the disassociation of higher ordered entities into smaller units. In order to determine the

oligomerization state of Tm1A in the regime between 0.4M-1.2M KCl, we used the ReFeyn mass photometer to analyze Tm1A at 500mM KCl. This resulted in a molecular weight of approximately 57 kDa (Figure 2.3), suggesting the base unit of Tm1A is a dimer (Dimer theoretical molecular weight is 58.4 kDa).

Our previous characterization of Tm1A (Hsiao et al., 2015) used actin purified from *Oryctalogus cuniculus* (rabbit) skeletal muscle actin, because it did not bind to *Acanthamoeba castellanii* actin, our non-muscle actin of choice for biochemical studies (unpublished observation). Here we show that Tm1A does in fact bind to purified S2 actin as well as rabbit, but not amoeba actins by TIRF microscopy (Figure 2.4).

Tm1A binding to pointed end tethered actin filaments

Our previous observations showed that Tm1A binds to actin filaments in a polarized manner (Hsiao et al., 2015). Specifically, we saw that at low concentrations of Tm1A, binding first occurred at or near the pointed, or slow growing, end of unbranched actin filaments *in vitro*. Filaments that were branched by the Arp2/3 complex and were therefore obstructed at the pointed end failed to incorporate Tm1A. To further test this idea, we established a microfluidic based, single filament assay (Figure 2.5A-B) with a variety of actin tethers to dissect this binding preference, and to test whether host actin contributed to this result. To test whether Tm1A could bind to filaments that were tethered at the pointed end we constructed stable biotin-phalloidin-actin seeds. We know that Tm1A cannot elongate on filaments that are completely tethered to the surface (unpublished observation), as it needs to wrap around filaments, so this assay was designed to mimic an obstruction to the pointed end, such as the Arp2/3 complex (Hsiao

et al., 2015). In order two differentiate regions of the filament, as well as test whether Tm1A had an affinity preference for labeled vs. dark actin we constructed ‘candy cane’ filaments. Specifically, we grew 1 uM Alexa647-S2 actin for four minutes under flow, switched to dark actin for the same amount of time, then again pulsed the 647 labeled actin (Figure 2.5C-3D). After allowing the last pulse to elongate for three to four minutes we added Tm1A to the chamber. We then quantified the first binding (i) location (Figure 2.5E), (ii) time from Tm1A enter the chamber to first binding event that formed a stable tropomyosin filament (Figure 2.5F). Very few of the initial binding events bound to the seed or pointed end of the filament, and for the most part these failed to elongate into the filament (Figure 2.5E). Likewise, there did not seem to be a preference for Tm1A binding to either a labeled or dark region of the filament (Figure 2.5E). We did see a dramatic shift of binding preference away from the pointed or older end of the filament compared to our previous paper (Hsiao 2015) and instead saw that the initial binding event of Tm1A was random with respect to filament position, regardless of Tm1A concentration (Figure 2.5E). We did see a concentration dependence in the time to the first binding event for Tm1A binding to our candy cane filaments, as well as Tm1A elongation rates (Figures 2.5F, 2.6A).

With these data in hand we can also begin to characterize the binding properties of the second tropomyosin strand. A rarely discussed topic due to the difficulties in observing this phenomenon with standard techniques. Our flow assay allows us to (i) distinguish the binding location of the second strand, (ii) ask whether this occurs on a similar or different location of the filament, (iii) whether the second binding event is likely to be in register with the first or second strand, (iv) whether the elongation kinetics are the

same or different for the two strands, (v) and whether the elongation kinetics differ when directed toward the barbed or pointed ends of the filament.

While we see that while elongation rates of Tm1A increase with increasing Tm1A concentration, the elongation rate is consistently faster toward the pointed end and slower toward the barbed end regardless of Tm1A concentration (Figure 2.6A). The elongation rates of the second strand do not significantly differ from the first strand, but also show polarized elongation favoring growth toward the pointed end of the filament (Figure 2.6A). At low concentrations of Tm1A we see that there are often multiple independent binding events of Tm1A (Fig 2.6B). As there are two strands of tropomyosin per actin filament, we ask whether the second binding event is likely to be in register with (same strand) or out of register (second strand) with the first binding event. At lower concentrations (187.5nM or less), the second binding event is on the first strand 25-35% of the time, but at all concentrations is more likely to be out of register with the first binding event (Figure 2.6C). Additionally, we see a large frequency of pausing events, which are not biased toward either direction, but happen most frequently at lower concentrations of Tm1A.

Tm1A binding to barbed end tethered actin filaments

Since tethering filaments to glass by their pointed end abolished Tm1A's polarized binding, we next reversed filament attachment to the glass surface by using tethers that specifically bind to the barbed end of filaments, namely mDia1 and Capping protein (Cp) (Figure 2.7A). mDia1 attached filaments grown in the presence of 250nM Tm1A almost exclusively exhibit binding of Tm1A at the pointed end of the filament (Figure 2.7B-D). These filaments tend to only remain associated with the mDia1 for ~5-10 min, and in this

time period the Tm1A typically does not elongate much past the initial binding site (Figure 2.7C-D). These actin filaments grew much faster due to the polymerase activity of mDia1 and also detached relatively quickly, therefore this failure to elongate into the filament could reflect a difference in the nucleotide state (age) of the filament as these filaments have a short lifetime; in all other Tm1A binding experiments, filaments were grown for at least 10 minutes prior to Tm addition.

When we instead pre-polymerized actin filaments, then added them to a chamber with Cp attached to the surface, we see that Tm1A still binds initially to or near the pointed end of the filaments, but also manages to coat the filaments (Fig 2.7E-F). Interestingly we fail to see any binding at or below 250nM Tm1A, a concentration at which pointed end tethered filaments were very rapidly bound and coated by Tm1A (Figures 2.6A, 2.7E-F). We wanted to test whether this failure to bind at low concentrations of Tm1A was due to being tethered at the barbed end, or reflected a difference in filaments capped by Cp. To test this, we looked at untethered and unattached filaments by TIRF microscopy in the presence or absence of Cp. Filaments were polymerized for 10 min, at which point Cp was added (or not) and then added Tm1A. We measured the time it took for Tm1A to bind to either capped or uncapped filaments across a range of concentrations. At all concentrations Tm1A bound much slower to filaments capped by Cp than uncapped filaments at the same concentration of Tm1A (Figure 2.7G). Additionally, the elongation of the Tm1A along the length of actin was much slower and was accompanied by more pausing than for uncapped filaments (Figure 2.7G).

Discussion

Studying actin binding proteins in the context of their host actins

To study the interaction of actin binding proteins (ABPs) to actin, it has long been accepted that actin purified from any source can be used because actin is so highly conserved. Comparative actin amino acid sequence analysis has shown that eukaryotic actins are over 80% conserved (Muller et al., 2005). Therefore, when needed, actin is purified from organisms that produce high quality, high concentrations of actin at an affordable price. Classically, actin from rabbit skeletal muscle (rabbit) was used to study muscle ABPs while *Acanthamoeba castellanii* non-muscle (amoeba) actin was used to study non-muscle ABPs.

In this chapter, we discovered that *Drosophila melanogaster* tropomyosin Tm1A can in fact detect the differences between rabbit skeletal muscle actin and *Acanthamoeba castellanii* non-muscle actin. Even more striking, *Drosophila melanogaster* tropomyosin Tm1A prefers muscle actin over non-muscle actin. This result suggests that ABPs and actins should be purified from the same model organism.

Tropomyosin stoichiometry

We have discovered that Tm1A is a dimer at one experimental concentration. However, in order to develop a detailed mechanistic model of how tropomyosin binds, we need to characterize tropomyosin's stoichiometry at different various concentrations. Analytical ultracentrifugation sedimentation equilibrium has proven to be impractical for Tm1A because we discovered that Tm1A forms aggregates during the course of the several days experiment. Recently, UCSF has acquired the Refeyn mass photometer. The mass photometer allows one to directly determine the stoichiometry of a protein,

including those of heterogeneous samples in under ten minutes. This equipment will serve as a great tool for future tropomyosin studies.

Tropomyosin binding is sensitive to how the actin filaments are tethered

Initial binding of Tm1A to actin filaments depends on the actin tether. One reason could be that pointed end tethers physically disrupt access to the actin filaments. We have previously shown that at low tropomyosin concentrations, Tm1A has pointed end preference to rabbit actin (Hsiao et al., 2015). In addition, when we added Tm1A to branched actin networks, Tm1A bound to the only free pointed end in the network, the mother filament. Therefore, it is possible that just simply capping the pointed end is enough to disrupt tropomyosin binding.

Another possibility is that pointed end tether used, the phalloidin-stabilized actin seed, changes the conformation of the actin filament pointed end. Phalloidin locks the actin seed in an ATP state. If the pointed end is in an ATP conformation vs. the normal ADP conformation, this could completely alter the structure of the actin filament and thus change how tropomyosin interacts with actin.

The last possibility is the age (nucleotide state) of the filament. For the experiments where tropomyosin Tm1A exhibited pointed-end preference, tropomyosin was introduced to actin filaments that were less than ten minutes old. In the phalloidin seed experiments where Tm1A had no end preference, filament were over 15 minutes old. This needs to be further tested to determine if the age of filaments can cause end preference.

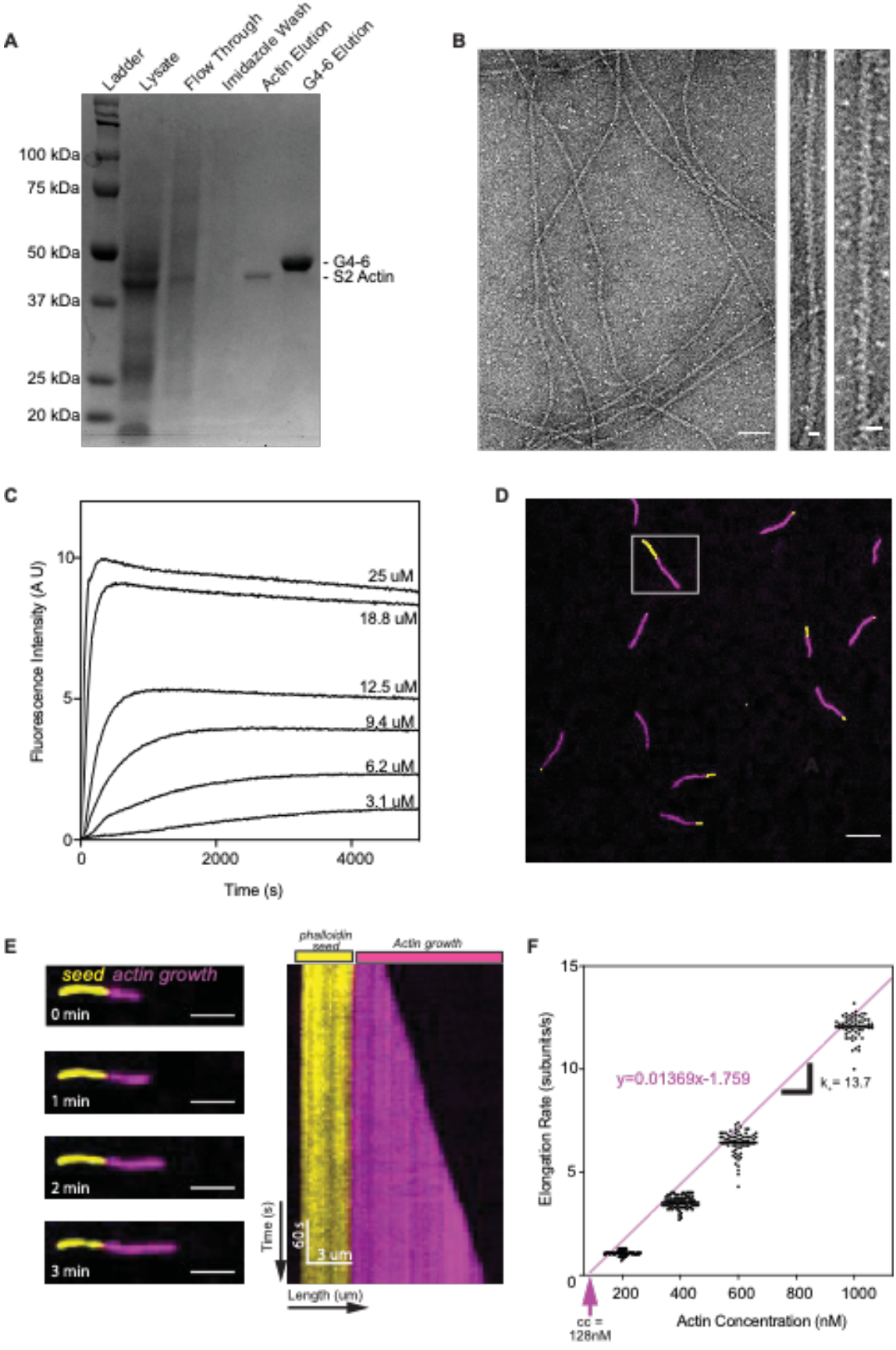
A
Ladder
Lysate
Flow Through
Imidazole Wash
Actin Elution
G4-6 Elution
100 kDa
75 kDa
50 kDa
37 kDa
25 kDa
20 kDa
- G4-6
- S2 Actin
B
C
Fluorescence Intensity (A.U)
25 uM
18.8 uM
12.5 uM
9.4 uM
6.2 uM
3.1 uM
Time (s)
D
E
seed actin growth
0 min
1 min
2 min
3 min
phalloidin seed
Actin growth
Time (s)
60 s
3 um
Length (um)
F
Elongation Rate (subunits/s)
y=0.01369x-1.759
k+= 13.7
cc = 128nM
Actin Concentration (nM)

Figure 2.1. Purification and characterization of D. melanogaster S2 actin.
(A) Coomassie stained SDS-PAGE gel showing the purification of S2 actin. Briefly, S2 cells were lysed and clarified (Lysate). The lysate was introduced into a nickel column and unbound material was collected (Flow Through). The nickel column was washed Gelsolin Wash Buffer to remove non-specific or weakly bound contaminants (Imidazole Wash). S2 actin was eluted using Actin Elution Buffer (Actin Elution). Gelsolin G4-6 was eluted with Gelsolin Elution Buffer (G4-6 Elution). (B) Negative Stain Electron Microscopy micrograph demonstrating that S2 actin forms actin filaments. (C) Pyrene actin polymerization assay demonstrates that S2 actin polymerization is concentration dependent. 40 μL S2 actin, 5% pyrene labeled, was incubated for 150 seconds with 10 μL of 10x ME buffer: 0.5 mM $MgCl_2$, 2 mM EGTA, pH 8. This actin mix was then combined with 50 μL of 2X polymerization buffer: 0.4 mM ATP, 1 mM DTT, 200 mM KCl, 2 mM $MgCl_2$, 2 mM EGTA, 10 mM HEPES, pH 7.0. (D) Representative TIRF image showing actin polymerizing (magenta) from biotin-phalloidin actin seeds (yellow). Image was background subtracted using a rolling ball with a radius of 7 pixels. (E) Left side. Actin filament montage of filament highlighted in D demonstrating actin filament elongation. Right side. Kymograph showing more detailed elongation of actin filament. (F). Elongation rates plotted as a function of actin concentration.

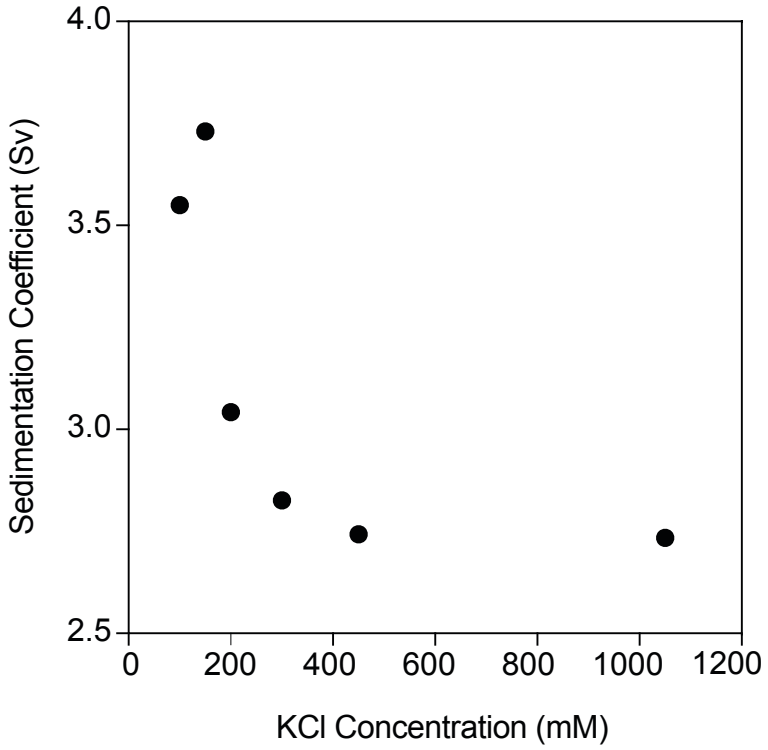

Figure 2.2. Sedimentation velocity analytical ultracentrifugation of tropomyosin Tm1A.
Sedimentation velocity demonstrates that the sedimentation coefficient of tropomyosin Tm1A decreases with increasing KCl concentration. 1.2 μM Tm1A conjugated with Alexa Fluor 568 in tropomyosin buffer (10 mM Imidazole, 0.5 mM TCEP, pH 7.0) with the desired salt concentration. Absorbance at OD_{575} was measured at 40000 rpm. Data was analyzed with SEDFIT.

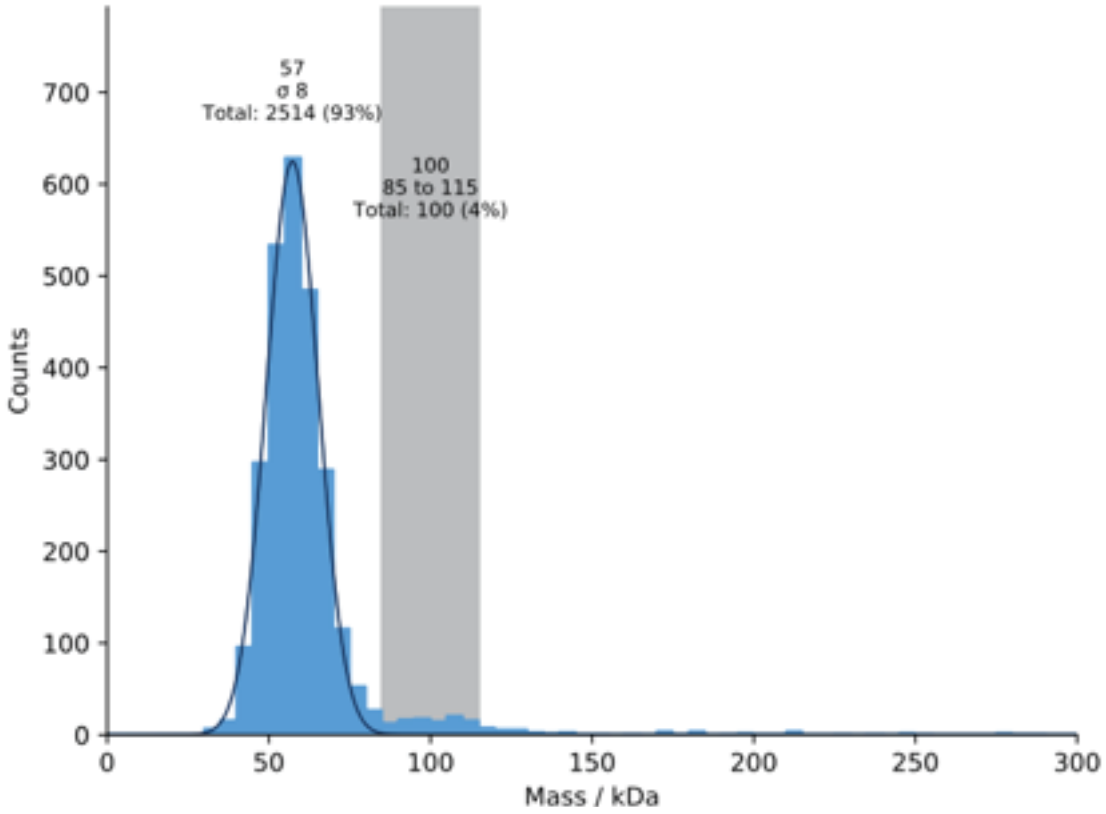

Figure 2.3. Refeyn mass photometer reveals Tropomyosin Tm1A is a dimer.
62.5 nM Tm1A was diluted in tropomyosin buffer with the following composition: 10 mM Imidazole, 100 mM KCl, 0.5 mM TCEP, pH 7.0) Data acquisition and analysis was automated by Refeyn software.

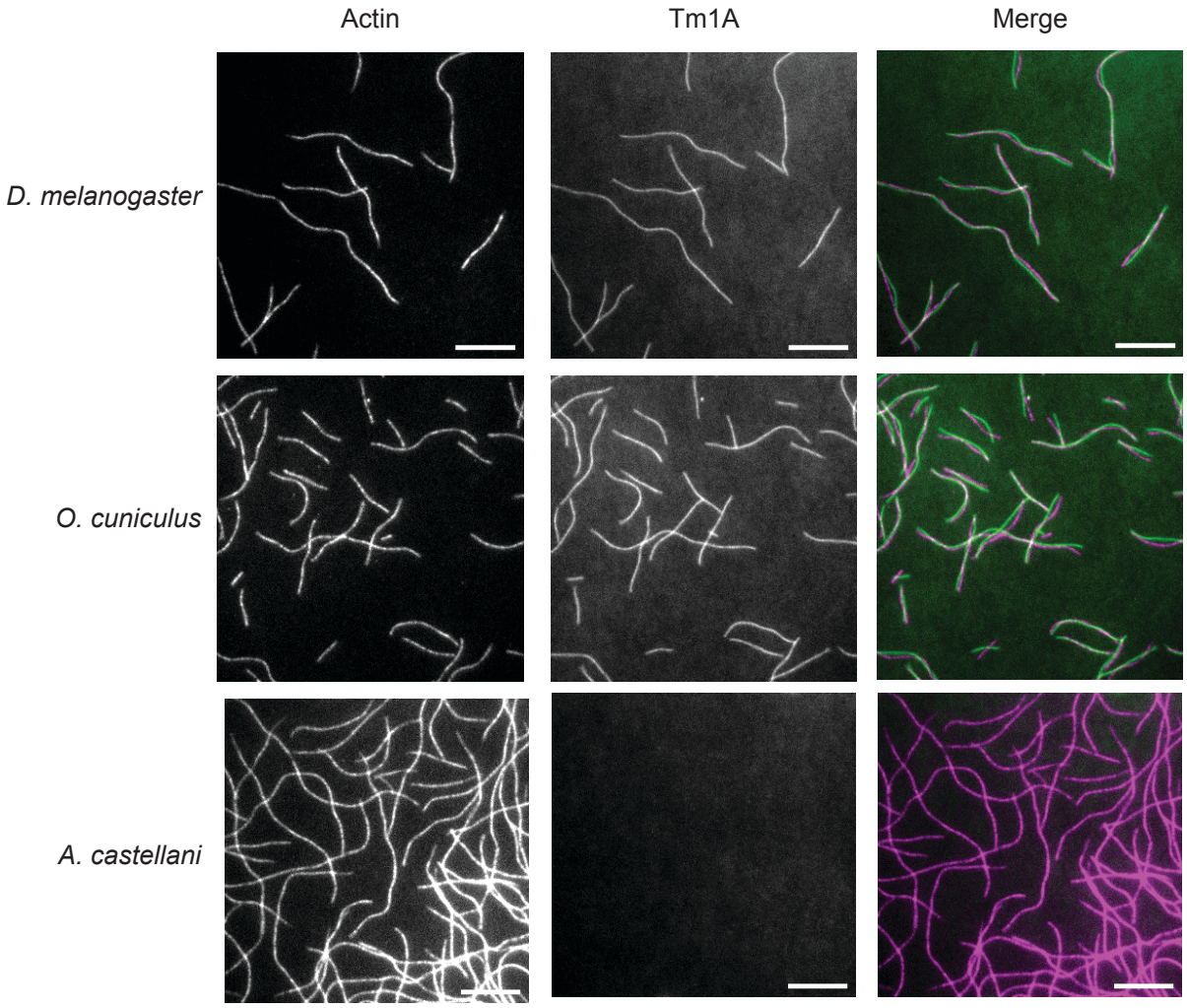

Figure 2.4. Tropomyosin Tm1A binding to actin filaments is dependent on the actin source.
Representative TIRF images for Tm1A (2nd column, green) binding to actins (1st column, magenta) from *D. melanogaster*, *O. cuniculus*, and *A. castellanii*. 1 μm of Tm1A (100% labeled with Alexa Fluor 488) was mixed with 1 μm actin (10% labeled with Alexa Fluor 647) in the presence of TIRF buffer.

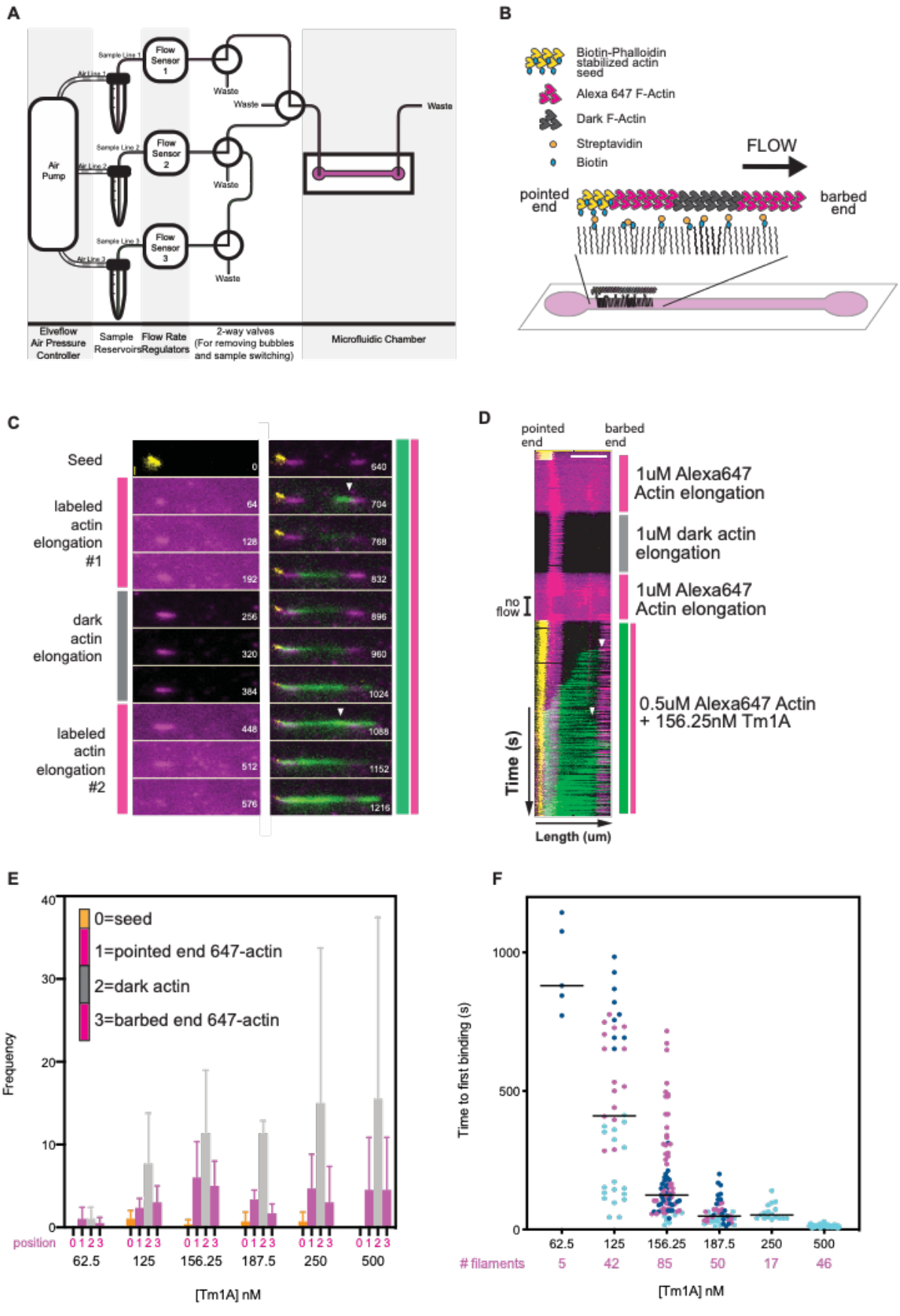
A
Flow Sensor 1
Flow Sensor 2
Flow Sensor 3
Waste
Air Pump
Elveflow Air Pressure Controller
Sample Reservoirs
Flow Rate Regulators
2-way valves (For removing bubbles and sample switching)
Microfluidic Chamber
B
Biotin-Phalloidin stabilized actin seed
Alexa 647 F-Actin
Dark F-Actin
Streptavidin
Biotin
FLOW
pointed end
barbed end
C
Seed
labeled actin elongation #1
dark actin elongation
labeled actin elongation #2
D
pointed end
barbed end
1uM Alexa647 Actin elongation
1uM dark actin elongation
1uM Alexa647 Actin elongation
no flow
0.5uM Alexa647 Actin + 156.25nM Tm1A
Time (s)
Length (um)
E
0=seed
1=pointed end 647-actin
2=dark actin
3=barbed end 647-actin
Frequency
position
[Tm1A] nM
F
Time to first binding (s)
filaments
[Tm1A] nM

Figure 2.5. Microfluidics coupled with TIRF microscopy reveals tropomyosin Tm1A initial binding location on actin filaments and time to first binding.
(**A**) Cartoon representation of the Elveflow microfluidic system coupled with two-way valves for reliable switching between biochemical conditions. (**B**) Scheme of pointed-end tethered actin filaments growing on passivated glass surfaces under microfluidic flow. (**C**) Left side. Montage of an actin filament assembled with a pointed-end labeled segment (64-192 s), a dark middle segment (256-384 s), and then a barbed-end labeled segment (448-576 s) under 30 μL/min microfluidic flow. Right side. Tm1A elongation on actin filaments. White arrowheads denote where the start site of Tm1A's first strand and second strand, respectively. (**D**) Kymograph of the same actin filament in C. White arrowheads denote where the start site of Tm1A's first strand and second strand, respectively. (**E**) Location of Tm1A's initial binding site on actin filaments. (**F**) Tm1A's time to first binding on actin filaments.

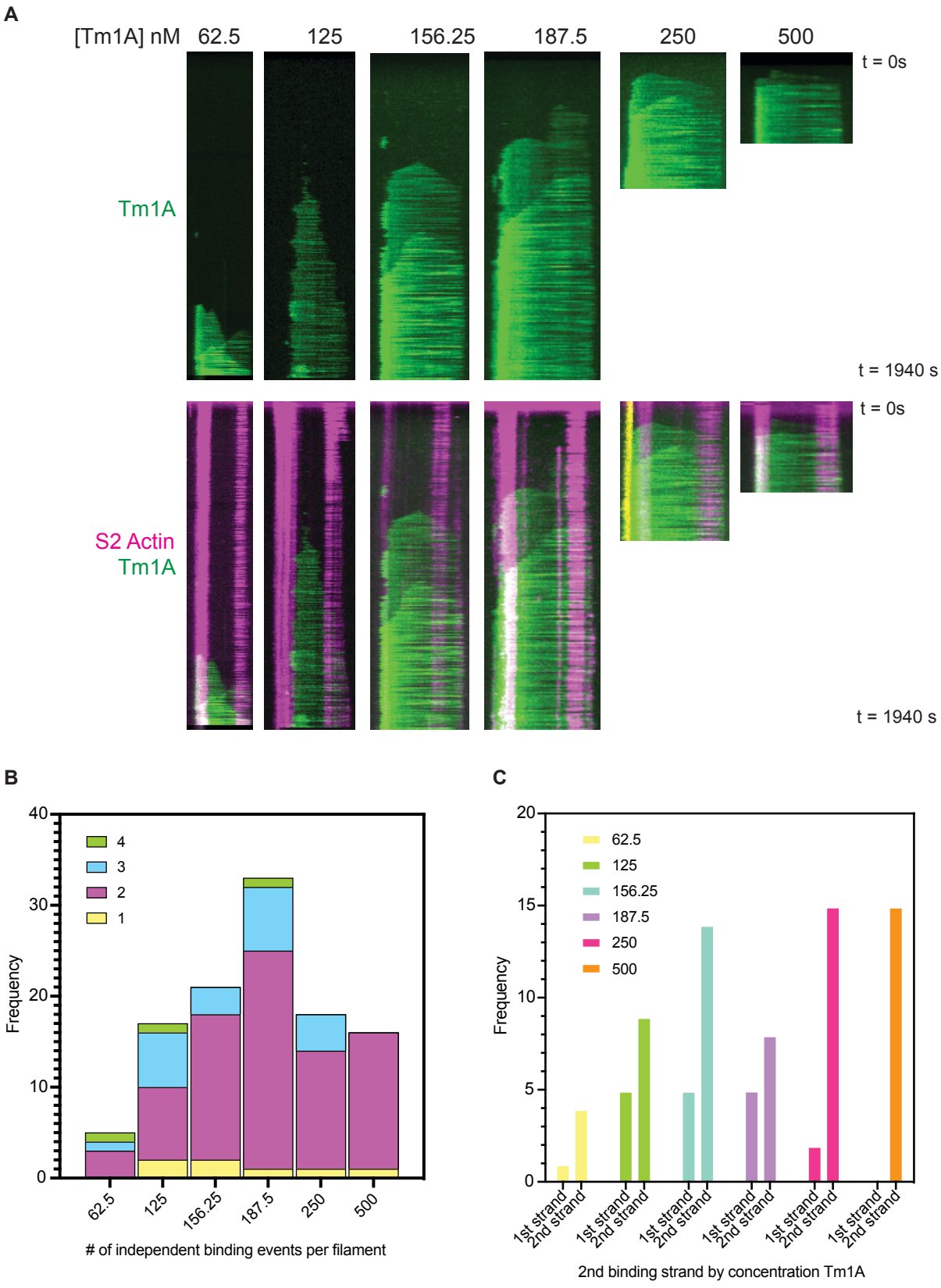
A
[Tm1A] nM
62.5
125
156.25
187.5
250
500
t = 0s
Tm1A
t = 1940 s
t = 0s
S2 Actin
Tm1A
t = 1940 s
B
Frequency
40
30
20
10
0
4
3
2
1
62.5
125
156.25
187.5
250
500
# of independent binding events per filament
C
Frequency
20
15
10
5
0
62.5
125
156.25
187.5
250
500
1st strand
2nd strand
2nd binding strand by concentration Tm1A

Figure 2.6. Microfluidics coupled with TIRF microscopy reveals tropomyosin Tm1A concentration dependence of Tm1A binding and dynamics.
(**A**). Kymographs of tropomyosin Tm1A (green) binding to S2 actin filaments (magenta) at various Tm1A concentrations. (**B**) Number of independent Tm1A binding events per actin filament. Independent binding events are defined as Tm1A binding that is not the result of Tm1A end-to-end polymerization. For this analysis, the actin filament is broken down into 4 segments, 1 being the pointed end and 4 being the barbed end. (**C**) Determining if the second independent binding event is in register with (same strand) or out of register with (second strand) the first binding event.

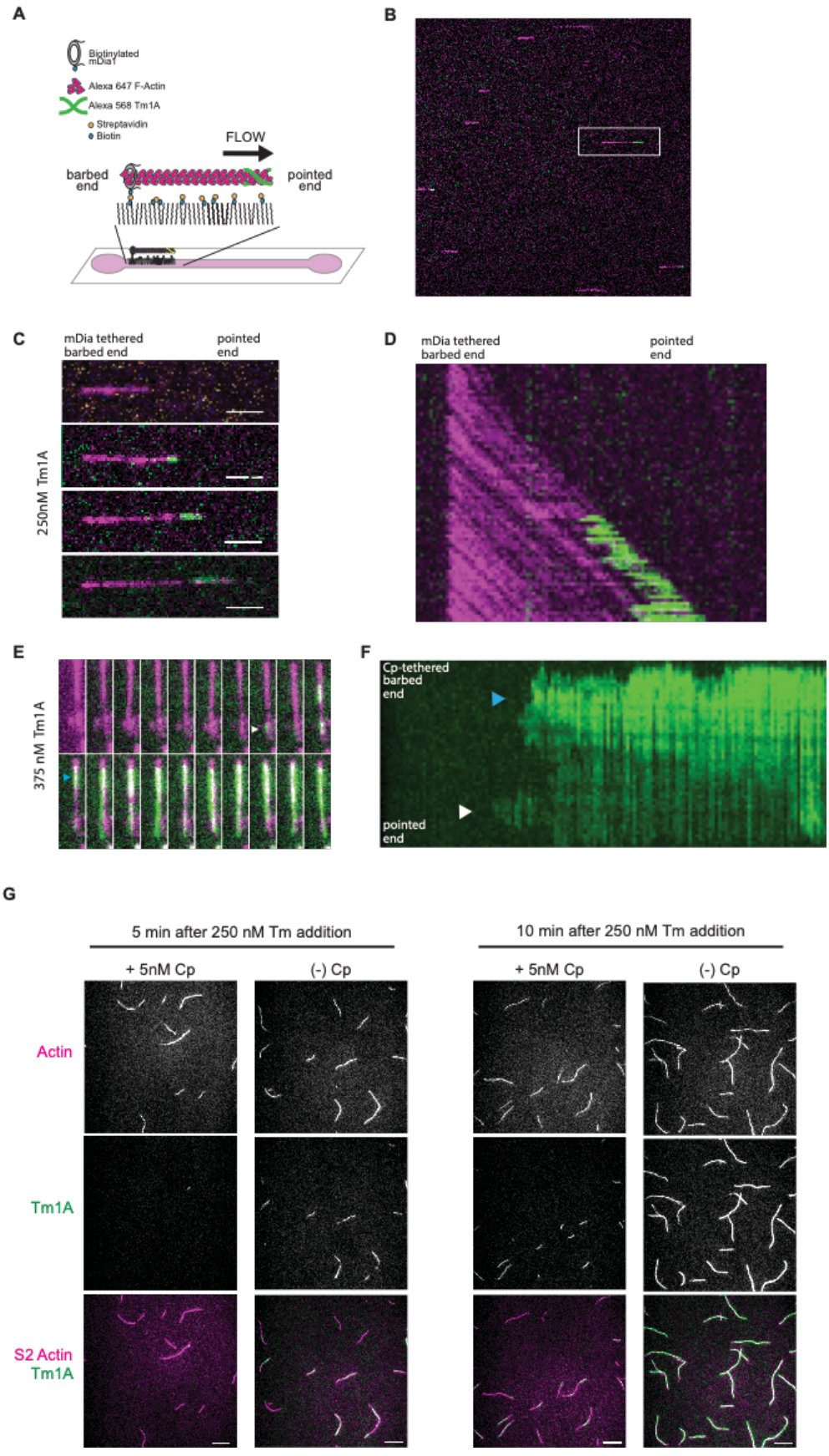
A
Biotinylated mDia1
Alexa 647 F-Actin
Alexa 568 Tm1A
Streptavidin
Biotin
FLOW
barbed end
pointed end
B
C
mDia tethered barbed end
pointed end
250nM Tm1A
D
mDia tethered barbed end
pointed end
E
375 nM Tm1A
F
Cp-tethered barbed end
pointed end
G
5 min after 250 nM Tm addition
10 min after 250 nM Tm addition
+ 5nM Cp
(-) Cp
+ 5nM Cp
(-) Cp
Actin
Tm1A
S2 Actin
Tm1A

Figure 2.7. Tropomyosin Tm1A has strong pointed end preference to actin filaments with unperturbed pointed ends.
(**A**) Scheme of barbed-end tethered actin filaments growing on passivated glass surfaces under microfluidic flow. (**B**) Representative TIRF image of tropomyosin Tm1A (green) binding to mDia1-tethered actin filaments (magenta). (**C**) Montage of filament highlighted in B. (**D**) Kymograph of filament highlighted in B. (**E**) Montage of Tm1A (green) binding to capping protein tethered actin filaments (magenta). (**F**) Tropomyosin Tm1A kymograph of filament shown in E. White arrowhead denotes first binding site, while blue arrowhead denotes second binding site. (**G**) Tm1A prefers to bind to actin filaments that not capped with capping protein. Cp represents capping protein.

Materials and Methods

Protein Purification and labeling

His_6-Gelsolin G4-6

His_6-Gelsolin G4-6 in the pCold vector was gratefully donated by Shin'ichi Ishiwata. The vector was transformed into Novagen's Rosetta2 *E. coli* competent cells. The transformation was plated on Luria Broth (LB) plates that contained 100 μg/mL carbenicillin (Carb) and 34 μg/mL chloramphenicol (Cam). To create a starter culture, a colony from the transformation was added to 70 mL of LB with 50 μg/mL Carb and 17 μg/mL Cam. Cultures were grown 30°C shaker at 200 rpm overnight.

10 mL of starter culture was added to every liter of Terrific Broth media containing 50 μg/mL Carb and 17 μg/mL Cam. The cultures were allowed to reach OD_{600} =1.8. The cultures were placed in 15°C ice baths for 30 min. 1 mM IPTG was added to the cells and allowed to induce in 15°C shaker overnight. Cells were harvested, flash frozen, and stored in -80°C for future use.

E. Coli cells were resuspended in Lysis Buffer (10 mM Tris, 50 mM KCl, 5 mM $CaCl_2$, 1 mM ATP, 1 mM BME, 1 mM PMSF, 1X Roche EDTA free protease inhibitor cocktail, pH 8.0). The cells were lysed using the Avestin C5 Emulsiflex and lysate was separated from cell debris by centrifugation at 167000 x g for 1 hour at 4°C. Lysate was loaded onto GE HisTrap excel columns. Columns were washed with Gelsolin Wash Buffer (10 mM Tris, 50 mM KCl, 5 mM $CaCl_2$, 1 mM ATP, 1 mM BME, 25 mM Imidazole, pH 8.0) and Gelsolin was eluted with Gelsolin Elution Buffer (10 mM Tris, 50 mM KCl, 5 mM $CaCl_2$, 1 mM ATP, 1 mM BME, 200 mM Imidazole, pH 8.0). Gelsolin was desalted into Wash Buffer with 1 mM DTT.

Native Drosophila melanogaster non-muscle Actin

Drosophila melanogaster S2 cells were seeded at a density of 2 x 10^6 cells/mL in SF 900 II media in sterile glass Erlenmeyer flasks with filtered caps and grown in 25ºC shaker until cells reached 10-15 x 10^6 cells/mL. S2 cells were harvested, flash frozen, and stored at -80°C for future use. S2 cells were resuspended in Actin Lysis Buffer (50mM Tris, 5mM $CaCl_2$, 1mM ATP, 1mM DTT, 5ug/mL aprotinin, 15 ug/mL benzamidine, 10ug/mL leupeptin, 5 ug/mL pepstatin, 40ug/mL Soybean Trypsin Inhibitor, 1mM PMSF, pH 8.0). Cells were lysed using Avestin C5 Emulsiflex. 50mM KCl was immediately added to lysate and 4mg of fresh Gelsolin G4-6 was added for every gram of S2 cells. Lysate with Gelsolin was incubated overnight at 4°C.

Lysate was separated from large cell debris by centrifugation at 167000 x g for 1 hour at 4°C. Residual debris was removed by centrifugation at 300000 x g for 1 hour at 4°C. Lysate was loaded onto GE HisTrap excel columns. Columns were washed with Gelsolin Wash Buffer (defined in Gelsolin section) followed by equilibration of Wash Buffer without imidazole. Actin was eluted with Actin Elution Buffer (10mM Tris, 50mM KCl, 1mM EGTA, 1mM ATP, and 0.5mM DTT, pH 8.0). Gelsolin was eluted using Elution Buffer (defined in Gelsolin section).

Actin fractions were pooled and polymerized by 10x MEH Buffer and $MgCl_2$ to a final concentration of 1x and 2 mM, respectively. Actin was allowed to polymerize for 4 hours at room temperature. Polymerized actin was pelleted by centrifugation at 278000 x g for 20 min at 4°C. Actin pellet was resuspended and dialyzed against Buffer A for several days.

Actin was pelleted by centrifugation at 278000 x g for 15 min at 4°C to remove aggregates. Actin was gel filtered using GE Superdex S200 and stored in dialysis buffer that was exchanged every two days until needed.

Acanthamoeba castellanii non-muscle actin

Acanthamoeba castellanii (amoeba) was cultured in autoclaved home-made amoeba medium with the following composition: 7.5 g/L proteose peptone, 7.5 g/L yeast extract, 15 g/L glucose, 0.2 mM methionine, 3 mM KH_3PO_4, 10 μM $CaCl_2$, 1 μM $FeCl_3$, 0.1 mM $MgSO_4$, 1 mg/L thiamine, 0.2 mg/L biotin, 0.01 mg/L vitamin B12. Amoeba were grown in 18 L glass carboys with moderate bubbling of humidified air until their optical density plateaued. Cells were harvested by centrifugation at 4500 x g for 5 min at 4°C. Amoeba cell pellets were washed with Wash Buffer (10 mM Tris, 150 mM NaCl, pH 8.0).

After cells were pelleted again, amoeba were resuspended in 1 mL of extraction buffer (10 mM Tris, 11.6% sucrose, 1 mM EGTA, 1 mM ATP, 5 mM DTT, 30 mg/L benzamidine, 5 mg/L pepstatin A, 10 mg/L leupeptin, 40 mg/L soybean trypsin inhibitor, 1 mM PMSF, pH 8.0) per gram of amoeba. Cells were lysed using the Parr Bomb at 400 psi, 5 min. Cell debris were removed by centrifugation at 5,000 x g for 10 min at 4°C. Supernatant was further clarified at 100,000 x g for 2 hours at 4°C.

Clarified supernatant was added to DEAE resin equilibrated in column buffer (10 mM Tris, 0.2 mM $CaCl_2$, 30 mg/L benzamidine, 0.5 mM ATP, 0.5 mM DTT, pH 8.0) and loaded onto an XK50 column. Column was washed with 1L of column buffer, Actin was eluted using a 2L linear gradient from 0 to 600 mM KCl. Final concentrations of 2 mM $MgCl_2$ and 1 mM ATP were added to the actin fractions to polymerize actin. Fractions were allowed to polymerize at room temperature for 4 hours. Cleanest fractions were

pooled and spun down using a centrifuge at 100,000 x g for 2 hours at 4°C. Actin pellet was resuspended in Buffer A and dialyzed for 2-4 days to depolymerize actin. Actin was gel filtered using a GE Superdex S200 Gel Filtration column. Best fractions were pooled and constantly dialyzed against Buffer A until needed.

Rabbit skeletal muscle actin

10 grams of rabbit skeletal muscle acetone powder (Pel-Freez Biologicals) was resuspended in 200 mL Buffer A and stirred for 30 min at 4°C. Muscle powder resuspension centrifuged at 16000 x g for 1 hour at 4°C and then supernatant was filtered through cheesecloth to remove muscle powder and precipitates. Actin was polymerized by adding a final concentration of 1x KMEH, 0.1 mM ATP. Actin was polymerized for 1 hour at room temperature and 1 hour at 4°C. Actin was spun down at 180000 x g for 2 hours at 4°C. Actin pellet was resuspended and dialyzed against Buffer A for 5 days. Actin was gel filtered via a GE Superdex S200 column and stored by constantly dialyzing against Buffer A at 4°C until needed.

Labeling actin with maleimide-conjugated or iodoacetamide-conjugated Dyes

Actin in Buffer A was pre-reduced with 2mM DTT for 2 hours at 4°C. Actin was buffer-exchanged into Labeling Buffer (5mM Tris, 0.1mM $CaCl_2$, 0.2mM ATP, pH 7.0) using PD-10 column. To polymerize 27μM actin, 10x KMEH was added to a final concentration of 1x. Actin was allowed to polymerize for 30 min at room temperature. 4 molar excess of maleimide-functionalized Alexa dyes was added to polymerize actin. Reaction was incubated overnight at 4°C.

Reaction was quenched with 10mM DTT. Dye aggregates were removed by centrifugation at 10000 x g for 15 min. Polymerized Actin was pelleted by centrifugation

at 278000 x g for 15 min. Actin was resuspended in Buffer A. Actin was gel filtered using GE Superdex S200 to remove excess dye. Actin was stored in Buffer A and was continuously dialyzed against fresh Buffer A until needed.

Drosophila melanogaster Tropomyosin Tm1A Labeling and Quantification

His_6-SUMO-MAS-Tm1A was overexpressed in *E. Coli* BL-21s (DE3) expression cells. Cells were grown in Terrific Broth media containing 100 μg/mL carbenicillin until OD_{600} = 0.8. Cells were induced with 1 mM IPTG in 37°C shaker for 4-5 hours. Cells were harvested, flash frozen, and stored at -80°C until needed. Cells were thawed and resuspended in Tm Lysis Buffer (50 mM Tris, 500 mM KCl, 5 mM BME, 1mM PMSF, 1x Roche EDTA-free Protease Inhibitor cocktail, pH 7.5). Cells were lysed using Avestin C5 Emulsiflex and lysate was cleared by centrifugation at 167000 x g at 4°C for 1 hour. Lysate was applied to GE HisTrap excel column. Column was washed with Tm Wash Buffer (10mM Tris, 500 mM KCl, 5 mM BME, 10 mM Imidazole, pH 7.5). Tm1A was eluted with Tm Elution Buffer (10mM Tris, 500 mM KCl, 5 mM BME, 500 mM Imidazole, pH 7.5). Best fractions were pooled and then His-tagged SUMO Protease was added. Tm1A was dialyzed against HA Binding buffer (5 mM Potassium Phosphate, 500 mM KCl, 0.5 mM TCEP, pH 7.5)

Tm1A was applied to a BioRad hydroxyapatite CHT Type I cartridge. Tm1A was eluted with a gradient that started with 100% HA Binding Buffer and 0% HA Elution Buffer (200mM Potassium Phosphate, 500mM KCl, 0.5mM TCEP, pH 7.5) and gradually increased to 0% HA Binding Buffer and 100% HA Elution Buffer. Cleanest tropomyosin fractions were pooled and gel filtered using GE Superdex S200 column via Tm Gel Filtration Buffer (10mM Tris, 500mM KCl, 0.5mM TCEP, pH 7.5). Tm1A was concentrated

and flash frozen in Tm Gel Filtration Buffer + 20% Glycerol. Protein was stored at -80°C until needed.

For labeling, Tm1A was pre-reduced with 2 mM DTT for 2 hours at 4°C. Tm1A was buffer-exchanged into Tm Gel Filtration Buffer without TCEP using PD-10 columns. 4 molar excess of maleimide-functionalized Alexa dyes were added to the tropomyosins. Reactions were incubated overnight at 4°C for 100% labeling. Reaction was quenched with 10 mM DTT. Dye aggregates were removed by centrifugation at 280000 x g for 15 min. Tm1A was gel filtered using GE Superdex S200 to remove excess dye and protein aggregates. Tm1A were stored in Tm Gel Filtration Buffer + 20% Glycerol until needed.

All unlabeled and AlexaFluor488-labeled tropomyosins were quantified using SYPRO Ruby protein gel stain as these tropomyosins contain no endogenous tryptophans and have very few tyrosines for accurate protein quantification at UV absorbance at 280 nm.

Drosophila melanogaster Profilin

His_6-SUMO-Profilin was overexpressed in *E. Coli* BL-21 Stars (DE3) expression cells. Cells were grown at 37°C in TB media containing 100 μg/mL carbenicillin until OD_{600} = 0.8. Cells were induced with 0.5 mM IPTG in 18°C shaker overnight. Cells were harvested, flash frozen, and stored at -80°C until needed.

Cells were thawed and resuspended in Profilin Lysis Buffer (50mM Tris, 150mM KCl, 1mM BME, 1mM PMSF, 1X Roche EDTA-free Protease Inhibitor cocktail, pH 8.0). Cells were lysed using Avestin C5 Emulsiflex and lysate was cleared by centrifugation at 180000 x g at 4°C for 1 hour. Clarified lysate was added to a GE HisTrap excel column equilibrated with Profilin Lysis Buffer. Column was washed Profilin Wash Buffer (10 mM

Tris, 150 mM KCl, 1 mM BME, pH 8.0) and then eluted with a gradient starting with 100% Profilin Wash Buffer and 0% Profilin Elution Buffer (10 mM Tris, 150 mM KCl, 1mM BME, 200 mM Imidazole), eventually ending with 0% Profilin Wash Buffer and 100% Profilin Elution Buffer. Best fractions were pooled and then His-tagged SUMO Protease was added. Profilin was dialyzed against Profilin Dialysis Buffer (10 mM Tris, 150 mM KCl, 5 mM BME, pH 8.0) overnight at 4°C.

Profilin's cleaved tag and SUMO Protease was removed by reapplying the protein over a HisTrap excel column equilibrated with Profilin Dialysis Buffer. The flow through was applied to a GE Superdex S200 Gel Filtration column. Pure Fractions were dialyzed against Profilin Storage Buffer (10 mM HEPES, 0.5 mM TCEP, 50% Glycerol, pH 7.0) overnight at 4°C. Profilin was flash frozen and stored at -80°C until needed.

Drosophila melanogaster Capping Protein

Capping Protein in pETDUET (Alpha subunit = wild type. Beta subunit = His_{10}-TEV-SNAP-Beta) was overexpressed in *E. Coli* BL-21 Stars (DE3) expression cells. Cells were grown at 37°C in Terrific Broth media containing 100 μg/mL carbenicillin until OD_{600} = 0.8. Cells were induced with 0.5 mM IPTG in 18°C shaker overnight. Cells were harvested, flash frozen, and stored at -80°C until needed.

Cells were thawed and resuspended in CP Lysis Buffer (50 mM Tris, 300 mM KCl, 1 mM BME, 1 mM PMSF, 1x Roche EDTA-free Protease Inhibitor cocktail, pH 8.0). Cells were lysed using Avestin C5 Emulsiflex and lysate was cleared by centrifugation at 180000 x g at 4°C for 1 hour. Clarified lysate was added to a GE HisTrap excel column equilibrated with CP Lysis Buffer. Column was washed CP Wash Buffer (10 mM Tris, 300 mM KCl, 1 mM BME, pH 8.0) and then eluted with a gradient starting with 100% CP Wash

Buffer and 0% CP Elution Buffer (10 mM Tris, 300 mM KCl, 1 mM BME, 300 mM Imidazole, pH 8.0), eventually ending with 0% Profilin Wash Buffer and 100% Profilin Elution Buffer. Best fractions were pooled and then His-tagged SUMO Protease was added. Profilin was dialyzed against CP Dialysis Buffer (10 mM Tris, 50 mM KCl, 5 mM BME, pH 8.0) overnight at 4°C.

Profilin's cleaved tag and SUMO Protease was removed by reapplying the protein over a GE HisTrap excel column equilibrated with CP Mono Q Buffer (10 mM Tris, 50 mM KCl, 5 mM BME, pH 8.0). The flow through was applied through a Mono Q column and eluted with a gradient of 50-500 mM KCl. Capping protein was gel filtered via a GE Superdex S200 Gel Filtration column. Pure Fractions were dialyzed against CP Storage Buffer (10 mM Tris, 50 mM KCl, 1 mM DTT, 50% Glycerol, pH 8.0) overnight at 4°C. Profilin was flash frozen and stored at -80°C until needed.

Escherichia coli BirA

His_6-MBP-BirA in pET vector was overexpressed in *E. Coli* Rosetta2 (DE3) expression cells. Cells were grown at 37°C in Terrific Broth media containing 50 μg/mL kanamycin until OD_{600} = 0.8. Cells were induced with 1 mM IPTG in 18°C shaker overnight. Cells were harvested, flash frozen, and stored at -80°C until needed.

Cells were thawed and resuspended in BirA Lysis Buffer (25 mM Tris, 200 mM KCl, 2 mM BME, 1 mM PMSF, 1x Roche EDTA-free Protease Inhibitor cocktail, pH 8.0). Cells were lysed using Avestin C5 Emulsiflex. Lysate was cleared by centrifugation at 180000 x g at 4°C for 1 hour. Clarified lysate was added to a HisTrap excel column equilibrated with BirA Lysis Buffer. Column was washed BirA Wash Buffer (25 mM Tris, 200 mM KCl, 2 mM BME, 20 mM Imidazole, pH 8.0) and then eluted with a gradient

starting with 100% CP Wash Buffer and 0% CP Elution Buffer (25 mM Tris, 200 mM KCl, 2 mM BME, 400 mM Imidazole, pH 8.0), eventually ending with 0% Profilin Wash Buffer and 100% Profilin Elution Buffer. Best fractions were applied to a GE Desalting 26/10 column equilibrated in BirA Storage Buffer (25 mM Tris, 200 mM KCl, 0.5 mM TCEP). BirA was used immediately or spiked to 20% Glycerol, flash frozen, and stored at -80°C until needed.

Mus musculus (Mouse) mDia1

GST-mDia1(549-1255 AA)-AVI in pGEX-6P-2 was overexpressed in *E. Coli* Rosetta2 (DE3) expression cells. Cells were grown at 37°C in TB media containing 50 μg/mL carbenicillin and 17μg/mL chloramphenicol until OD_{600} = 0.8. Cells were induced with 0.3 mM IPTG at 18°C overnight. Cells were harvested, flash frozen, and stored at -80°C until needed.

Cells were thawed and resuspended in mDia1 Lysis Buffer (50 mM Sodium Phosphate, 150 mM KCl, 1 mM DTT, 10% Glycerol, 1 mM PMSF, 1x Roche EDTA-free Protease Inhibitor cocktail, pH 8.0). Cells were lysed using Avestin C5 Emulsiflex. Lysate was cleared by centrifugation at 180000 x g at 4°C for 1 hour. Clarified lysate was added to a GSTrap FF column equilibrated with mDia1 Lysis Buffer. Column was washed mDia1 Lysis Buffer and then eluted Elution Buffer (20 mM Sodium Phosphate, 150 mM KCl, 1 mM DTT, 10 mM reduced Glutathione, 10% Glycerol). Best fractions were pooled and mixed with His-tagged-MBP-BirA. mDia1 was dialyzed against mDia1 Dialysis Buffer (10 mM HEPES, 150 mM KCl, 0.5 mM Biotin, 1 mM ATP, 1 mM $MgCl_2$, 1 mM TCEP, pH 7.4) overnight at 4°C.

BirA was removed by applying the protein over a HisTrap excel column equilibrated with mDia1 Storage Buffer (10 mM HEPES, 150 mM KCl, 1 mM TCEP, pH 7.4). The flow through was applied to a GE Desalting 26/10 column to remove excess biotin. Desalted fractions were concentrated, spiked to 20% Glycerol, flash frozen, and stored at -80°C until needed.

Negative Stain Electron Microscopy

Samples were prepared by applying 2.5 μL of protein sample to 200mesh, Formvar carbon coated glow discharged grids and incubating for 30 seconds. Grids were washed three times in protein buffer, blotting between washes. Grids were stained three times with 0.75% uranyl formate, blotting between applications. For the last staining step, grid was incubated in stain for 30 seconds. Micrographs were taken with a Technai T12 microscopy with 120 kV voltage and a magnification of 48000. Images were taken with a Gatan 4k x 4k charge-coupled device camera.

Pyrene Actin Polymerization Assay

40 μL actin (5% Pyrene labeled) was mixed with 10 μL 10x ME buffer (0.5 mM $MgCl_2$, 2 mM EGTA, pH 8.0) and incubated for 150 seconds. The actin mix was then combined with 50 μL of 2X polymerization buffer: 0.4 mM ATP, 1 mM DTT, 200 mM KCl, 2 mM $MgCl_2$, 2 mM EGTA, 10 mM HEPES, pH 7.0. The reaction was immediately recorded using a BioTek Synergy 4 Plate reader at 8 second intervals for 75 minutes.

Mass Photometry

Samples were applied to a Refeyn mass photometer that was calibrated with a native protein standard mixture. Movies were acquired using Acquire software for 180 seconds. Data was analyzed on Discover software.

Sedimentation Velocity Analytical Ultracentrifugation

1.2 μM Tm1A conjugated with Alexa Fluor 568 in tropomyosin buffer (10 mM Imidazole, 0.5 mM TCEP, pH 7.0) at various concentrations of KCl were set up in sedimentation velocity cells. Absorbance at OD_{575} was measured at 40000 rpm for 5 hours. Data was analyzed with SEDFIT

Preparation of Biotin-Phalloidin Actin Seeds

5 μM of actin in fresh Buffer A was mixed with enough 10x KMEH buffer and 500 mM TCEP to reach a final concentration of 1x KMEH and 1 mM TCEP, respectively. Actin was allowed to polymerize at room temperature for 30 min. 2x Phalloidin Buffer (1x KMEH, 5 mM Alexa Fluor-labeled Phalloidin, 5 mM Biotin Phalloidin, 1 mM ATP, 5 mM TCEP) was added 1:1 to the actin mix. Phalloidin-actin was pelleted using centrifugation at 280000 x g for 30 min. The pellet was light washed by pipetting in and immediately removing 500 μL of Seed Buffer (1x KMEH, 1 mM ATP, 5 mM TCEP pH 7.0). The pellet was then resuspended in enough Seed Buffer to make 5 μM actin.

TIRF Chamber Assembly

Preparation of Glass

Microscope slides were sonicated for 20 minutes in 3 M KOH and then rinsed with copious amounts of Milli-Q water. Slides were dried using argon or nitrogen gas. Slides were stored in a slide box at room temperature for future use. High precision coverslips were etched on one side with a diamond pen to distinguish the coverslip sides. The unetched side underwent silanization and PEGylation as described below:

Coverslips were sonicated for 20 minutes in 3 M KOH and then rinsed with copious amounts of Milli-Q water. The coverslips were dried using a custom-made coverslip spinner with Teflon rotors (check Mullins lab website for parts list). The coverslips were further dried by baking at 70°C for 30 minutes. The baked coverslips were then plasma treated in a Harrick Plasma Cleaner at high power for 5 minutes. Immediately following plasma treatment, (3-Glycidloxypropyl) trimethoxysilane was sandwiched between two clean coverslips, sandwiches were placed into weighing jars, and the weighing jars were baked for 70°C for 1 hour.

Silanized coverslips were rinsed with HPLC-grade acetone to remove excess silane. 75 µL of 300 mg/mL NH_2-PEG-5000-methoxy with 3% NH_2-PEG-5000-Biotin in HPLC-grade acetone was sandwiched between two coverslips, coverslip sandwiches were placed into weighing jars, and the weighing jars were baked for 70°C for 4-5 hours. Coverslips were washed with copious amounts of Mili-Q water, dried using the coverslip spinner, and stored under vacuum at -20°C until used.

TIRF Chamber Assembly for experiments that do not require flow

Laser cutter was used to cut three channels into 3M double-sided tape (9474LE 300LSE). These channels served as chambers for three separate experiments. To assemble the TIRF chamber, the laser cut tape was sandwiched with a passivated coverslip and a clean microscope slide.

Microfluidic Chamber Assembly

Laser cutter was used to cut a microfluidic channel into 3M double-sided tape (9474LE 300LSE). This tape was applied to a clean microscope slide. Using the laser-cut tape inlet and outlets as a guide, a Dremel with a diamond drill bit was used to create the inlet and outlet holes. IDEX Nanoports were glued using epoxy to the inlet and outlets (opposite side of the tape), serving as an easy and reliable method for microfluidic line connection. The chamber assembly was cured at room temperature for several hours. A passivated coverslip was applied to the remaining double-sided tape side. The completed chamber was baked in a 70°C oven for 10 minutes.

TIRF Microfluidics

A two-way valve was connected to each microfluidic chamber (chamber with 1 inlet and 1 outlet), serving as a bubble removal tool when connecting/disconnecting lines and during solution addition. This assembly was connected to the Elveflow OB1 pressure controller with flow sensors. For experiments requiring solution switching, the assembly shown in Figure2.5A was used.

TIRF Imaging and Reaction Setup

Visualizing actin filaments using TIRF Microscopy was performed using a modified protocol as outlined in Hansen and Mullins (2010) and Kuhn and Pollard (2005). Briefly, TIRF chambers were blocked with 5 mg/mL K-Casein and 0.5 mg/mL B-Casein in K100MEH with TCEP (100 mM KCl, 1 mM $MgCl_2$, 1 mM EGTA, 10 mM HEPES, 0.5 mM TCEP, pH 7.0). After 3 minutes, the chamber was washed with K100MEH with TCEP, removing excess blocking reagents.

To prepare the reaction mix, actin and tropomyosin (concentrations used described in figure legends) were combined with TIRF buffer with the final composition of: 200 units/mL catalase, 110 units/mL glucose oxidase, 20 mM glucose, 0.2 mM ATP, 0.2% methylcellulose cP400, 40 mM 2-Mercaptoethanol, 100mM KCl, 1mM $MgCl_2$, 1mM EGTA, 10mM HEPES, pH 7.0.

For microfluidic TIRF experiments, chambers were blocked and washed with TIRF buffer as described for methylcellulose experiments. Chambers were then incubated with 50 nM Streptavidin for 5 min and then actin tether (mDia1, Capping Protein, or Seeds) for 5 min. Actin and tropomyosin were combined with Profilin and Microfluidic TIRF buffer with the final composition: 200 units/mL catalase, 110 units/mL glucose oxidase, 20 mM glucose, 0.2 mM ATP, 2-Mercaptoethanol, 100mM KCl, 1mM $MgCl_2$, 1mM EGTA, 10mM HEPES, pH 7.0.

References

Balasubramanian, M., Bi, E., Glotzer, M. (2004). Comparative analysis of cytokinesis in budding teast, fission yeast and animal cells. *Current Biology*, 14(18), R806-R818.

Dalby-Payne, J., O'Loughlin, E., Gunning, P. (2003). Polarization of Specific Tropomyosin isoforms in gastrointestinal epithelial cells and their impact on CFTR at the apical surface*. Molecular Biology of the Cell*, 14(11), 4365-4375.

D'Ambrosio, M., Vale, R. (2010). A whole genome RNAi screen of Drosophila S2 cell spreading performed using automated computational image analysis. *The Journal of Cell Biology*, 191(3), 471-478.

Ecken, J., Heissler, S., Pathan-Chhatbar, S., Manstein, D., Raunser, S. (2016). Cryo-EM structure of a human cytoplasmic actomyosin complex at near-atomic resolution. *Nature*, 534(7609), 724-728.

Goins, L., Mullins, R. (2015). A novel tropomyosin isoform functions at the mitotic spindle and golgi in Drosophila*. Molecular Biology of the Cell,* 26(13), 2491-2504.

Gumbiner, B. (1996). Cell Adhesion: The molecular basis of tissue architecture and morphogenesis*. Cell,* 84(3), 345-357.

Hansen, S., Zuchero, J., Mullins, R. (2013). Cytoplasmic actin: Purification and single molecule assembly assays. *Methods Molecular Biology*, (Clifton, N.J.) 1046(), 145-170.

Heath, J., Dunn, G. (1978). Cell to substratum contacts of chick fibroblasts and their relation to the microfilament system. A correlated interference-reflexion and high-voltage electron-microscope study. *Journal of cell science,* 29(), 197-212.

Holmes, K., Popp, D., Gebhard, W., Kabsch, W. (1990). Atomic model of the actin filament. *Nature*, 347(6288), 44-49.

Hsiao, J., Goins, L., Petek, N., Mullins, R. (2015). Arp2/3 complex and cofilin modulate binding of tropomyosin to branched actin networks. *Current Biology*, 25(12), 1573-1582.

Iwasa, J., Mullins, R. (2007). Spatial and temporal relationships between actin-filament nucleation, capping, and disassembly. *Current Biology*, 17(5), 395-406.

Kuhn, J., Pollard, T. (2005). Real-Time measurements of actin filament polymerization by Total Internal Reflection Fluorescence Microscopy. *Biophysical Journal,* 88(2), 1387-1402.

Mabuchi, I. (1994). Cleavage furrow: timing of emergence of contractile ring actin filaments and establishment of the contractile ring by filament bundling in sea urchin eggs. *Journal of cell science*, 107(Pt 7), 1853-62.

Muller, J., Oma, Y., Vallar, L., Friederich, E., Poch, O., Winsor, B. (2005). Sequence and comparative genomic analysis of actin-related proteins. *Molecular Biology of the Cell*, 16(12), 5736-5748.

Percival, J., Thomas, G., Cock, T., Gardiner, E., Jeffrey, P., Lin, J., Weinberger, R., Gunning, P. (2000). Sorting of tropomyosin isoforms in synchronized NIH 3T3 fibroblasts: Evidence for distinct microfilament populations. *Cell Motility and the Cytoskeleton*, 47(3), 189-208.

Pollard, T., Cooper, J. (2009). Actin, a central player in cell shape and movement. *Science*, 326(5957), 1208-1212.

Rogers, S., Rogers, G. (2008). Culture of Drosophila S2 cells and their use for RNAi-mediated loss-of-function studies and immunofluorescence microscopy. *Nature Protocols*, 3(4), 606-611.

Rogers, S., Wiedemann, U., Stuurman, N., Vale, R. (2003). Molecular requirements for actin-based lamella formation in Drosophila S2 cells. *The Journal of Cell Biology*, 162(6), 1079-1088.

Schevzov, G., Whittaker, S., Fath, T., Lin, J., Gunning, P. (2011). Tropomyosin isoforms and reagents. *BioArchitecture*, 1(4), 135-164.

Svitkina, T., Borisy, G. (1999). Arp2/3 complex and Actin Depolymerizing Factor/Cofilin in dendritic organization and treadmilling of actin filament array in lamellipodia. The Journal of Cell Biology, 145(5), 1009-1026.

Whitby, F., Phillips, G. (2000). Crystal structure of tropomyosin at 7 Ångstroms resolution. *Proteins: Structure, Function, and Bioinformatics*, 38(1), 49-59.

Yamada, Y., Namba, K., Fujii, T. (2020). Cardiac muscle thin filament structures reveal calcium regulatory mechanism. *Nature Communications*, 11(1), 153.

Chapter Three

Characterization of Drosophila tropomyosins Tm1J and Tm2A on Drosophila actin filaments

Contributions

Experiments

Protein constructs and protein purifications were performed by Johnny Rodriguez. Tropomyosin quantifications were performed by Natalie A. Petek-Seoane. Experiments for figures 1, 4, and 5 were performed equally by Johnny Rodriguez and Natalie A. Petek-Seoane. Experiments for figures 2 and 3 were performed by Johnny Rodriguez

Figure Production

Figure production for figures 1 and 4 were performed by Natalie A. Petek-Seoane. Figure production for figures 2, 3, and 5 were performed by Johnny Rodriguez. Cartoon drawing in figure 3 was made by Arthur Charles-Orszag.

Chapter writing

Writing for chapter was performed by Johnny Rodriguez.

Introduction

Actin is one of the most abundant proteins in eukaryotic cells. Actin monomers assemble into actin filaments, which in turn assemble into many different three-dimensional structures, each capable of performing a specialized function. These actin networks are involved in various cellular processes, such as maintenance of cell morphology (Pollard and Cooper, 2009), plasma membrane protrusion (Svitkina and Borisy, 1999; Iwasa and Mullins, 2007), production of cell adhesion (Heath and Dunn, 1978; Gumbiner, 1996), and assembly of a contractile ring that splits a cell into two during cell division (Mabuchi, 1994; Balasubramanian et al., 2004). Currently, it is widely believed that the key determinant that specifies which actin network will form are tropomyosins.

Although tropomyosins may play an important role in determining which actin network can form (Percival et al., 2000; Dalby-Payne et al., 2003), tropomyosins remain largely understudied. This is largely due to the fact that mammalian cells encode for four different tropomyosin genes, giving rise to over two dozen different tropomyosin isoforms (Schevzov et al., 2011). To circumvent the complexity of mammalian systems, we have chosen *Drosophila melanogaster* S2 cells for the study of tropomyosins because they only encode for three tropomyosin isoforms. In addition, S2 cells are easy to grow, are highly susceptible to gene inhibition using RNAi (Rogers and Rogers et al., 2008), and have well characterized actin networks (D'Ambrosio and Vale, 2010; Rogers et al., 2003; Iwasa and Mullins, 2007). Previously we have performed a thorough biochemical characterization of tropomyosin Tm1A (Chapter 1). We will now focus on the characterization of the other two tropomyosins: Tm1J and Tm2A.

Our lab recently discovered that tropomyosins Tm1J and Tm2A have some unique and some overlapping localizations (Goins and Mullins, 2015). In interphase, Tm1J colocalizes with Tm1A to lamellar actin networks. Tm1J also colocalizes with Tm2A to the actin networks around the Golgi. In addition, Tm1J localizes to centrosomes, kinetochores, and the central spindle.

Tropomyosins Tm1J and Tm2A influence cell cycle progression. During mitosis, Tm1J and Tm2A completely disperse from the Golgi upon nuclear envelope breakdown. Interestingly, when Tm1J and/or Tm2A are depleted, S2 cells pile up in G1 phase. When these tropomyosins are overexpressed, S2 cells accumulate in G2/M phase.

Despite the importance of tropomyosins Tm1J and Tm2A, we still do not understand how they assemble on actin filaments. Preliminary data from Jenny Hsiao demonstrated that tropomyosin Tm1J was not able to bind to rabbit skeletal muscle actin. Does Tm1J not bind because rabbit skeletal muscle actin was used or does Tm1J require a cofactor to help it bind actin filaments? In this chapter we investigate the binding of Drosophila Tm1J and Tm2A to Drosophila actin filaments.

Results

Tropomyosins Tm1J and Tm2A do not bind actin filaments

To study the interaction of *Drosophila melanogaster* tropomyosins Tm1J and Tm2A to *Drosophila melanogaster* S2 actin, we added methionine, alanine, and serine residues to the N-terminus of both Tm1J and Tm2A. These residues have been shown to restore the binding of unacetylated tropomyosins to actin filaments, thus mimicking the function of the N-terminal acetylation found on tropomyosins in *vivo* (Monteiro et al., 1994). These modified tropomyosins will now be referred to as Tm1J and Tm2A. To purify these tropomyosins, we used the N-terminal His_6-SUMO tag purification strategy (Catanzariti et al., 2004), which ultimately leaves no unnecessary amino acids at the N-Terminus.

Previously, we have identified that *Drosophila melanogaster* tropomyosin Tm1A's interaction with actin filaments depends on the species the actin is purified from (Chapter 1 and Jennifer Hsiao preliminary data). Therefore, our next question was to determine whether Tm1J and Tm2A binding depends on the actin source. Using TIRF microscopy, we discovered that Tm1J and Tm2A were also not able to bind rabbit skeletal muscle actin and *Acanthamoeba castellanii* non-muscle actin (Figures 3.1B-C). In conclusion, our results demonstrate that AS-Tm1J and AS-Tm2A do not bind actin, regardless of the actin source.

Tm1J and Tm2A fold into coiled-coil homodimers

One possibility is that Tm1J and Tm2A do not bind actin filaments because they are not properly folded. We first ran the amino acid sequence of the tropomyosins through COILS, a software which compares the tropomyosin sequences to a database of known

two-stranded coiled-coils. As expected, these tropomyosins are predicted to fold into classical coiled coils. We next used circular dichroism (CD) to confirm the presence of alpha helices, which in turn dimerize to form coiled coils. If either tropomyosin is not able to form alpha helices, it would strongly indicate that these tropomyosins are not forming coiled coils. Figure 3.2A shows the CD spectra for each tropomyosin. The spectra of Tm1J and Tm2A suggests both tropomyosins fold into mainly alpha helices.

To determine whether tropomyosin is forming dimers, we used analytical ultracentrifugation (AUC). AUC sedimentation equilibrium experiments suggest Tm1J and Tm2A are forming dimers (data not shown). All this data strongly suggests that Tm1J and Tm2A are indeed folding into their predicted structures and improper folding in not the reason why these tropomyosins are unable to bind actin filaments

We also used CD to reveal the melting curves for each tropomyosin to determine their thermal stabilities. Thermal stability can indicate whether a protein would be stable enough to survive in a cell. Interestingly, Tm1J seems more stable than Tm2A because Tm1J folding does not significantly change until about 45 °C, where the sharp unfolding transition begins (Figure 3.2B, left side). On the other hand, Tm2A seems to unfold significantly at temperatures as low as 25 °C (Figure 3.2B, right side), the temperature at which Drosophila S2 cells are generally grown at. Although Tm1J and Tm2A most likely form coiled coils, Tm1J is more stable than Tm2A.

Tropomyosin Tm1J/Tm2A heterodimers bind actin filaments

One idea is that Tm1J and Tm2A need to heterodimerize to bind actin filaments. Our lab has previously shown that eGFP-Tm1J and eGFP-Tm2A colocalize to actin networks surrounding the Golgi in *Drosophila melanogaster* S2 cells. When looking at the

sequence alignment of Tm1J and Tm2A, these tropomyosins have an identical N-terminus and are highly similar throughout the rest of the sequence. In addition, these two tropomyosins are the same length, making it possible to form a coiled coil without overhangs. Although there are no reports of tropomyosin heterodimers in non-muscle cells, tropomyosin heterodimers have been identified in muscle (Bronson and Schachat, 1982; Sanders et al., 1986; Gimona et al., 1995)

To test whether AS-Tm1J and AS-Tm2A can heterodimerize to bind actin, we took advantage of the phenomenon that tropomyosins unfold when heated to near boiling temperatures and can rapidly refold once the temperature has been brought down to room temperature. We first heated Tm1J to 70°C for 10 min and incubated at room temperature for 10 min. The refolded Tm1J was immediately introduced to actin filaments and the interaction was visualized using TIRF microscopy (Figure 3.3A, first row). In these conditions, Tm1J was still not able to bind actin filaments. We repeated the same experiment using Tm2A and saw the same result (Figure 3.3A, second row). We next mixed Tm1J and Tm2A together and introduced this mix to actin. AS-Tm1J and AS-Tm2A were not able to copolymerize onto actin filaments (Figure 3.3A, third row). Finally, we mixed AS-Tm1J and AS-Tm2A together, boiled to 70°C for 10 min, and then incubated at room temperature for 10 min. Strikingly, when we add this mixture to actin, Tm1J and Tm2A copolymerize on actin filaments (Figure 3.3A, fourth row). Upon close observation, we never saw an instance where Tm1J did not colocalize with Tm2A, suggesting they are copolymerizing. Taken together this data suggests that Tm1J and Tm2A heterodimerize and now gain the ability to bind actin filaments.

To determine whether Tm1J and Tm2A are forming heterodimers, we created a tandem affinity purification protocol to purify the heterodimer from *E. Coli* expression cells (Figure 3.3B). Briefly, Tm1J was N-terminally tagged with StrepTag-SUMO tag while Tm2A was N-terminally tagged with a His_6 tag-SUMO tag. These constructs were both placed into a pETDuet vector. The purification was performed in 500mM KCl to make sure that tropomyosins are not able to oligomerize. By removing the tropomyosins' ability to oligomerize, we can eliminate contaminating tropomyosin homodimers that may be interacting with the heterodimer. The purified heterodimer was labeled with a maleimide-conjugated dye and its interaction with actin filaments was visualized using TIRF. The purified Tm1J/Tm2A heterodimer was able to bind to actin filaments (Figure 3.3C). In summary, Tm1J and Tm2A can form heterodimers that are capable of binding to actin filaments.

We next sought to determine whether there is anything unique about the structure of the heterodimer. We first used circular dichroism to determine whether the heterodimer forms the alpha helices required to form the canonical tropomyosin coiled coil. According to the CD spectra, the heterodimer forms alpha helices (Figure 3.3D, left side). Next, we sought to determine whether the heterodimer is more stable than the Tm1J and Tm2A homodimers. To do this, we obtained a melting curve for the heterodimer and compared it to the melting curves of the Tm1J and Tm2A homodimers. Interestingly, the heterodimer melting curve is biphasic (Figure 3.3D, right side). The most likely possibility is that the heterodimer is actually a mixture of consisting of Tm1J/Tm2A heterodimer, Tm1J homodimer, and the Tm2A homodimer. Since Tm1J and Tm2A melt at slightly different temperatures, one could imagine that a mixture of these tropomyosins may lead to a

biphasic curve. In conclusion, the heterodimer secondary structure folds into alpha helices and the heterodimer is not significantly more stable than the homodimers.

Tm1J/Tm2A heterodimer binding to actin filaments depends on the actin source

As mentioned earlier, *Drosophila melanogaster* tropomyosin Tm1A binding to actin filaments depends on the organism the actin was purified from. Now that we discovered tropomyosin heterodimer Tm1J/Tm2A binds actin filaments, we wanted to ask whether heterodimer binding to actin filaments is also sensitive to the actin source. To answer this question, we used TIRF to visualize heterodimer binding to rabbit skeletal muscle actin and *acanthamoeba castellanii* actin (Figure 3.4). To our surprise, heterodimer Tm1J/Tm2A bound to both rabbit actin and amoeba actin. Taken together, this data demonstrates that the tropomyosin heterodimer is not sensitive to the source of actin.

Tm1A and Tm1J/Tm2A heterodimer copolymerize on actin filaments

In *Drosophila melanogaster* S2 cells, Tm1A and Tm1J/Tm2A segregate to different actin networks. During interphase, Tm1A localizes to the lamella and cell cortex, while Tm1J/Tm2A localizes to the actin network surrounding the Golgi. Do Tm1A and Tm1J/Tm2A have the innate ability to segregate to their own actin filaments or does some other protein or cytosolic factor segregate these proteins in S2 cells. We addressed this question by adding Tm1A and Tm1J/Tm2A to S2 actin and visualizing the outcome using TIRF (Figure 3.5). Interestingly, Tm1A and Tm1J/Tm2A copolymerize together on actin filaments. Interestingly, the fluorescence of Tm1A is brighter than the fluorescence of Tm1J/Tm2A. However, we cannot rule out whether this due to the fluorophores used. In conclusion, Tm1A and Tm1J/Tm2A do not have the innate ability to segregate to different actin filaments.

Discussion

For the very first time, we show that non-muscle tropomyosins can form heterodimers. Heterodimers provide one big advantage: increasing functional diversity. With the ability to associate into homodimers and heterodimers, tropomyosins monomers can form many different combinations of tropomyosins, allowing tropomyosins to have different biochemical properties and interact with different actin binding proteins without the need of an extra gene or splice variant. The discovery of heterodimers may help explain why some tropomyosins have poor cellular fluorescence signal when overexpressed (Goins and Mullins, 2015). This also means that those studying the complex tropomyosin library in mammalian will have orders of magnitude more complexity.

Why is tropomyosin heterodimer Tm1J/Tm2A capable of binding while Tm1J and Tm2A homodimers do not?

There are two possibilities as to why the Tm1J/Tm2A heterodimer can bind actin filaments, while the Tm1J and Tm2A homodimers do not: (1) The heterodimer has extra actin binding sites or just an overall high affinity for actin. (2) The heterodimer has stronger tropomyosin head to tail overlaps, allowing the tropomyosin to bind cooperatively to actin filaments. When looking at the tropomyosin sequences, most of the tropomyosin variability is at the C-terminus. Therefore, although it is likely that the C-terminus encodes for extra actin binding sites or higher affinity actin binding sites. I predict that the reason the heterodimer is able to bind to actin filaments is because tropomyosin can form stronger head to tail overlaps.

We also observed that the CD spectra of Tm2A had lower signal than any of the other tropomyosins we tested. One possibility is that the Tm2A is less stable than the Tm1J homodimer and then Tm1J/Tm2A heterodimer. This would favor the formation of the other two species. When looking at the tropomyosin fluorescence data in S2 Cells, we never saw Tm2A bind actin filaments on its own.

Tropomyosin Tm1J/Tm2A and tropomyosin Tm1A do not sort to different actin filaments

Unlike our observations in *Drosophila* S2 cells, we observed that tropomyosins Tm1A and heterodimer Tm1J/Tm2A do not segregate to their own actin filaments. This suggests that other proteins or factors are necessary to segregate tropomyosins. One possibility are formins, a class of actin nucleators and polymerases. The FH2 domains of some formins have been shown to interact with tropomyosins. Interestingly, it was shown that in yeast, mislocalization of a formin, led to the mislocalization of a tropomyosin. By having an actin nucleator determine which tropomyosins to recruit, this means that at the conception of the actin filament, formins can begin depositing tropomyosins.

Another possibility is tropomodulin. Tropomodulin is a protein that binds and caps the pointed end of actin filaments. Interestingly, tropomodulin contains two tropomyosin-binding sites, presumably one for each tropomyosin strand on the actin filament. Tropomodulins make sense for selecting which tropomyosin it needs at the birth of the actin filament. Unless tropomodulin can change the structural conformation of the entire actin filament, tropomodulin would need another factor to ensure the right tropomyosin is added downstream.

The last possibility is troponins, troponin is a calcium-binding protein complex that is known to play an important role in regulating the conformation of tropomyosins in

muscle cells. Interestingly, troponins interact with the overlap region of tropomyosins. In this way, troponins could control which tropomyosins are depositing by proofreading the tropomyosin overlap region. Recently, troponins have been discovered in non-muscle cells. Although these proteins appear to affect actin networks, their mechanism remains to be elucidated. Future work is required to identify the protein factor needed to sort tropomyosins.

The future of the tropomyosin field

We have discovered the mechanism for how all the *Drosophila melanogaster* tropomyosins in S2 cells bind actin filaments. The next big question is: What are the functional differences between the tropomyosins?

Each tropomyosin isoform is thought to recruit a unique subset of actin binding proteins by either having a unique conformation on actin filaments or through tropomyosins' unique protein sequences. To help answer these questions, a cryo-EM structure of Tm1A-coated actin filaments and Tm1J/Tm2A-coated actin filaments needs to be obtained to look for conformational differences between the tropomyosins. In addition, binding partners need to be identified. These experiments will help answer many of the burning questions about tropomyosin and as always, lead to exciting new questions

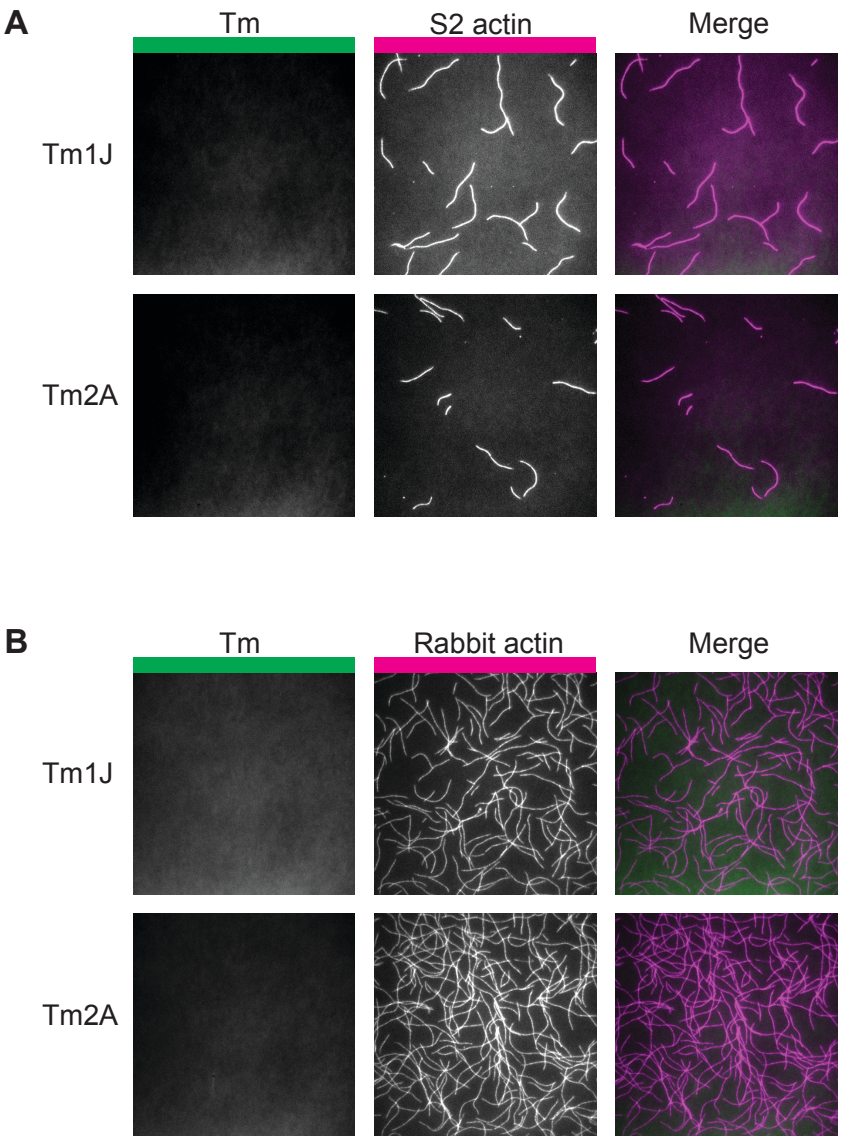
A
Tm
S2 actin
Merge
Tm1J
Tm2A
B
Tm
Rabbit actin
Merge
Tm1J
Tm2A
C
Tm
Amoeba actin
Merge
Tm1J
Tm2A

Figure 3.1. Drosophila tropomyosins Tm1J and Tm2A do not bind actin filaments, regardless of what species the actin originated from.
(**A, B, C**) Representative TIRF images for Tropomyosins (Tm, green) binding to actins (magenta) from *Drosophila melanogaster*, rabbit skeletal muscle, and *Acanthamoeba castellanii*. 1 μm of corresponding tropomyosin (100% labeled with Alexa Fluor 488) was mixed with 1 μm actin (10% labeled with Alexa Fluor 647) in the presence of TIRF buffer.

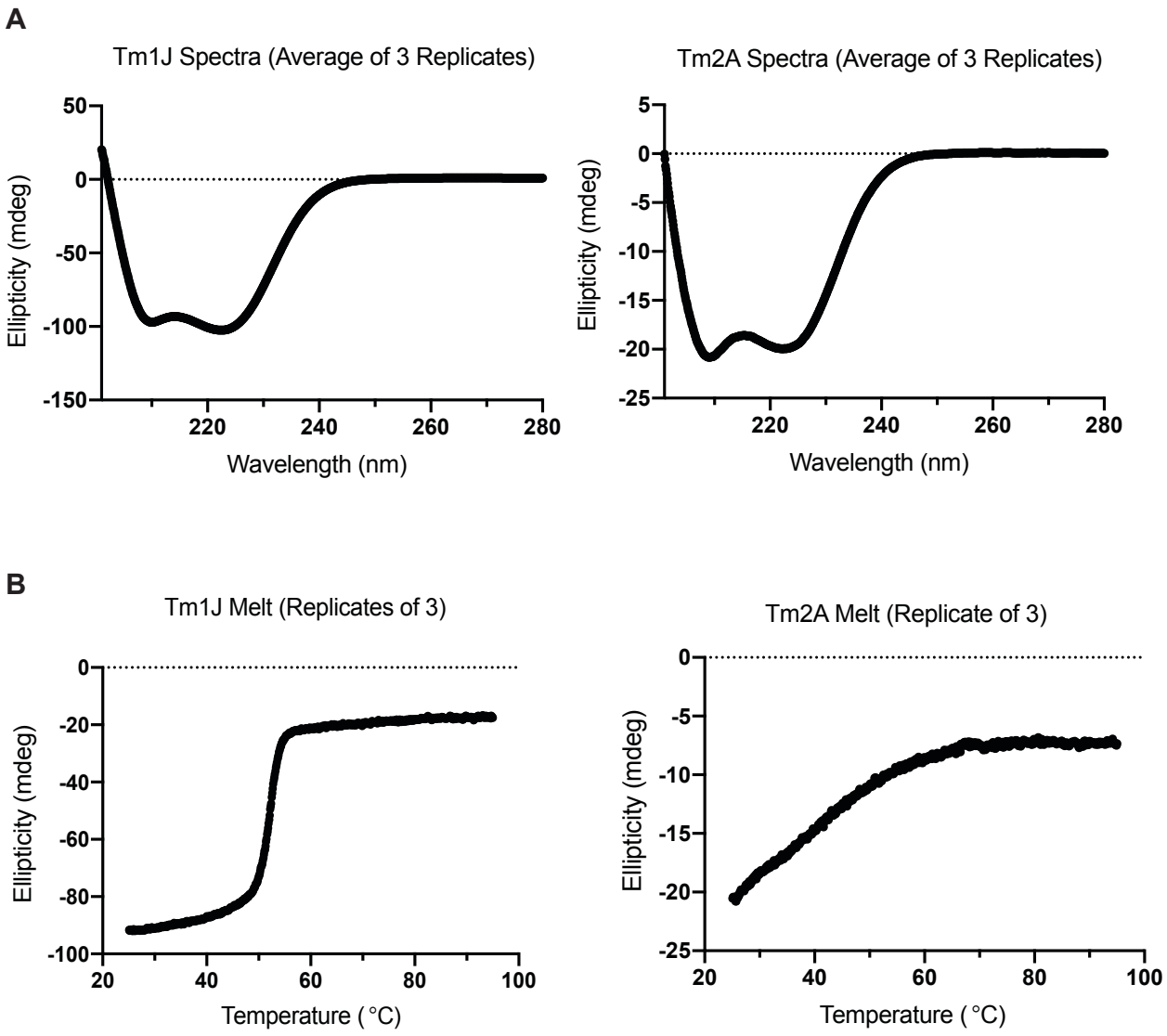

Figure 3.2. Tropomyosins Tm1J and Tm2A fold into coiled-coil homodimers. (**A**) Circular Dichroism spectra scan for each Tm1J and Tm2A show that these tropomyosins form canonical alpha helices. (**B**) Circular Dichroism melting curve of each Tm1J and Tm2A. Tropomyosin Tm1J's melt transition has a half max at 52 °C. Tm2A's melt transition has a half max at 41 °C.

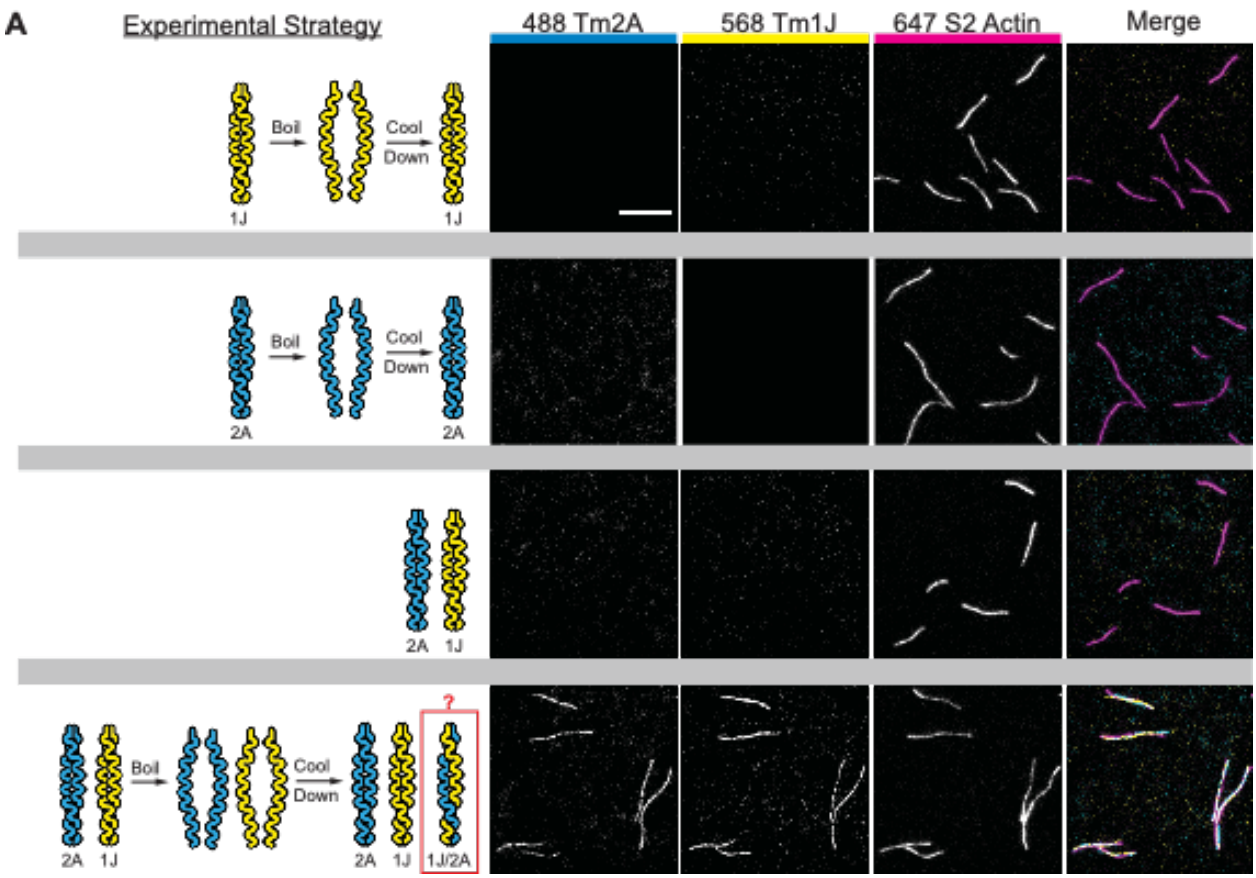
A
Experimental Strategy
488 Tm2A
568 Tm1J
647 S2 Actin
Merge
Boil
Cool Down
1J
1J
2A
2A
2A
1J
2A
1J
2A
1J
1J/2A
?

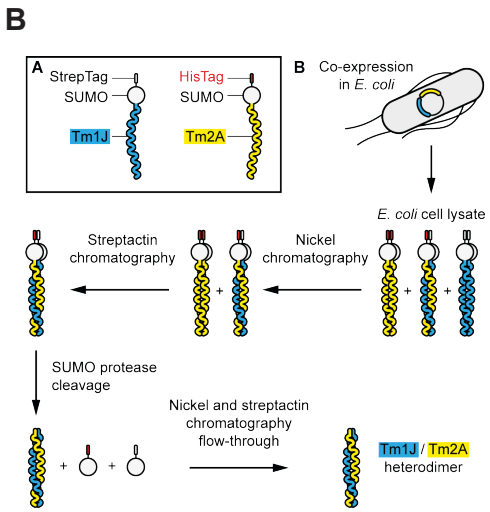
B
A
StrepTag
SUMO
Tm1J
HisTag
SUMO
Tm2A
B
Co-expression in E. coli
E. coli cell lysate
Streptactin chromatography
Nickel chromatography
SUMO protease cleavage
Nickel and streptactin chromatography flow-through
Tm1J / Tm2A heterodimer

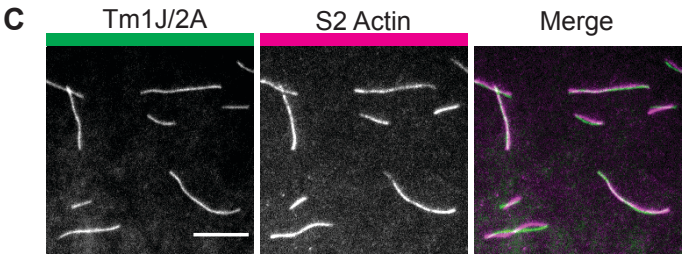
C
Tm1J/2A
S2 Actin
Merge

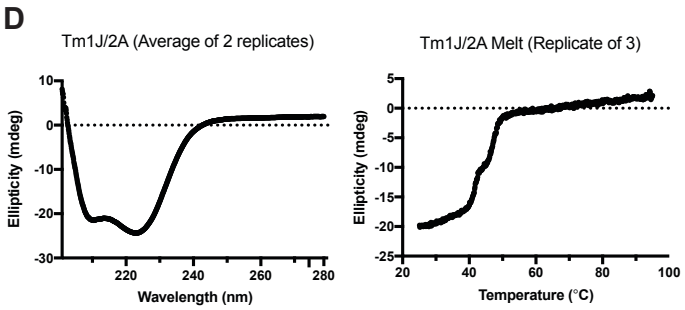
D
Tm1J/2A (Average of 2 replicates)
Ellipticity (mdeg)
10
0
-10
-20
-30
220
240
260
280
Wavelength (nm)
Tm1J/2A Melt (Replicate of 3)
Ellipticity (mdeg)
5
0
-5
-10
-15
-20
-25
20
40
60
80
100
Temperature (°C)

Figure 3.3. Heterodimerization of Tm1J and Tm2A is required for actin binding. (**A**) Left side is a cartoon representation detailing how tropomyosin(s) were handled for each experiment shown. When boiling was required for experiment, tropomyosins were boiled at 70 °C for 10 min and then incubated at room temperature for 10 min. Right side has representative TIRF microscopy images showing tropomyosins Tm1J and Tm2A only bind to S2 actin filaments when Tm1J and Tm2A are boiled and cooled down together. 500 nM S2 Actin, 10% Alexa Fluor 647 labeled (magenta), was mixed with 1 μm Tm2A, 100% Alexa Fluor 488 labeled (cyan), and/or 1 μm Tm1J, 100% Alexa Fluor 568 labeled (yellow), in the presence of TIRF buffer (Buffer composition in materials and methods). Images were taken 15 minutes into the experiment. Scale bar, 10 μm. Experiment was performed three times with two Tm1J preps, two Tm2A preps, and three separate S2 actin preps. (**B**) Cartoon representation of the tandem affinity purification strategy for tropomyosin heterodimer Tm1J/Tm2A. Purification was performed in 500 mM KCl to prevent oligomerization, which would compromise purity. (**C**) Representative TIRF images show purified Tm1J/Tm2A heterodimer (green) binds to S2 actin filaments (magenta). 1 μm Tm1J/Tm2A heterodimer (100% labeled with Alexa Fluor 568) was mixed with 1 μm S2 actin (10% labeled with Alexa Fluor 647) in the presence of TIRF buffer. Images were taken 15 min into experiment. Scale bar, 10 μm. (**D**) Circular Dichroism spectra scan of tropomyosin heterodimer Tm1J/Tm2A shows that tropomyosin forms canonical alpha helices (Left side). Circular Dichroism melting curve of tropomyosin heterodimer Tm1J/Tm2A demonstrates the heterodimer has biphasic melting properties (Right side). First melt transition has a half max at 42 °C and the second melt transition at 47 °C.

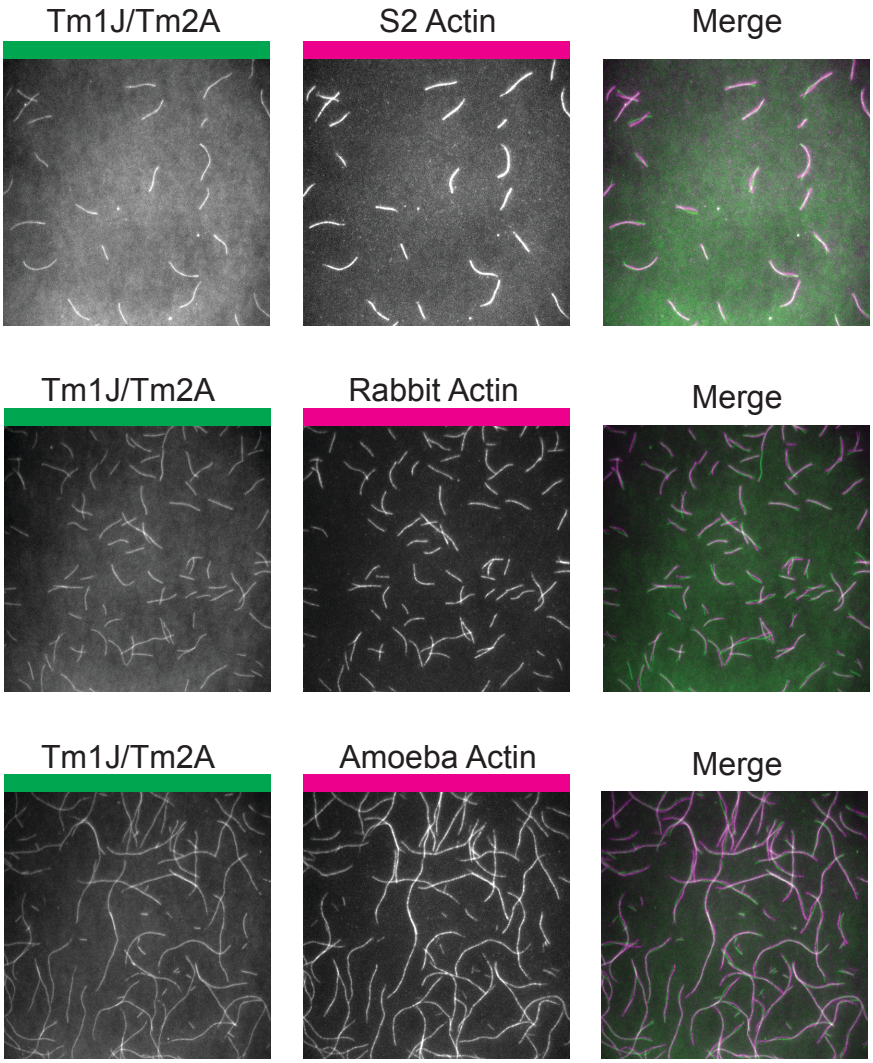

Figure 3.4. Tropomyosin heterodimer Tm1J/Tm2A is not sensitive to the actin source.
Representative TIRF images show purified Tm1J/Tm2A heterodimer (green) binds to S2 actin, Rabbit actin, and Amoeba actin (magenta). 1 μm Tm1J/Tm2A heterodimer (100% labeled with Alexa Fluor 568) was mixed with 1 μm actin (10% labeled with Alexa Fluor 647) in the presence of TIRF buffer. Images were taken 15 min into experiment.

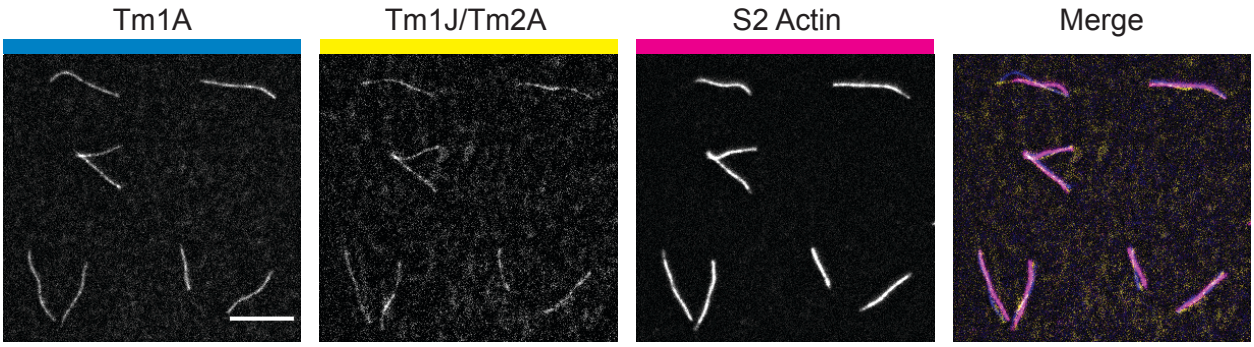

Figure 3.5. Tropomyosin heterodimer Tm1J/Tm2A copolymerizes with tropomyosin Tm1A on actin filaments.
Representative TIRF images show Tm1A (cyan) and Tm1J/Tm2A heterodimer (yellow) binding to S2 actin filaments (magenta). 500 nM Tm1A (100% labeled with Alexa Fluor 488) and 500 nM Tm1J/Tm2A heterodimer (100% labeled with Alexa Fluor 568) was mixed with 1 μm S2 actin (10% labeled with Alexa Fluor 647) in the presence of TIRF buffer. Scale bar, 10 μm.

Materials and Methods

Protein Purification and labeling

His_6-Gelsolin G4-6

His_6-Gelsolin G4-6 in the pCold vector was gratefully donated by Shin'ichi Ishiwata. The vector was transformed into Novagen's Rosetta2 *E. coli* competent cells. The transformation was plated on Luria Broth (LB) plates that contained 100 μg/mL carbenicillin (Carb) and 34 μg/mL chloramphenicol (Cam). To create a starter culture, a colony from the transformation was added to 70 mL of LB with 50 μg/mL Carb and 17 μg/mL Cam. Cultures were grown 30°C shaker at 200 rpm overnight.

10 mL of starter culture was added to every liter of Terrific Broth media containing 50 μg/mL Carb and 17 μg/mL Cam. The cultures were allowed to reach OD_{600} =1.8. The cultures were placed in 15°C ice baths for 30 min. 1 mM IPTG was added to the cells and allowed to induce in 15°C shaker overnight. Cells were harvested, flash frozen, and stored in -80°C for future use.

E. Coli cells were resuspended in Lysis Buffer (10 mM Tris, 50 mM KCl, 5 mM $CaCl_2$, 1 mM ATP, 1 mM BME, 1 mM PMSF, 1X Roche EDTA free protease inhibitor cocktail, pH 8.0). The cells were lysed using the Avestin C5 Emulsiflex and lysate was separated from cell debris by centrifugation at 167000 x g for 1 hour at 4°C. Lysate was loaded onto GE HisTrap excel columns. Columns were washed with Gelsolin Wash Buffer (10 mM Tris, 50 mM KCl, 5 mM $CaCl_2$, 1 mM ATP, 1 mM BME, 25 mM Imidazole, pH 8.0) and Gelsolin was eluted with Gelsolin Elution Buffer (10 mM Tris, 50 mM KCl, 5 mM

$CaCl_2$, 1 mM ATP, 1 mM BME, 200 mM Imidazole, pH 8.0). Gelsolin was desalted into Wash Buffer with 1 mM DTT.

Native Drosophila melanogaster non-muscle Actin

Drosophila melanogaster S2 cells were seeded at a density of 2 x 10^6 cells/mL in SF 900 II media in sterile glass Erlenmeyer flasks with filtered caps and grown in 25ºC shaker until cells reached 10-15 x 10^6 cells/mL. S2 cells were harvested, flash frozen, and stored at -80°C for future use. S2 cells were resuspended in Actin Lysis Buffer (50mM Tris, 5mM $CaCl_2$, 1mM ATP, 1mM DTT, 5ug/mL aprotinin, 15 ug/mL benzamidine, 10ug/mL leupeptin, 5 ug/mL pepstatin, 40ug/mL Soybean Trypsin Inhibitor, 1mM PMSF, pH 8.0). Cells were lysed using Avestin C5 Emulsiflex. 50mM KCl was immediately added to lysate and 4mg of fresh Gelsolin G4-6 was added for every gram of S2 cells. Lysate with Gelsolin was incubated overnight at 4°C.

Lysate was separated from large cell debris by centrifugation at 167000 x g for 1 hour at 4°C. Residual debris was removed by centrifugation at 300000 x g for 1 hour at 4°C. Lysate was loaded onto GE HisTrap excel columns. Columns were washed with Gelsolin Wash Buffer (defined in Gelsolin section) followed by equilibration of Wash Buffer without imidazole. Actin was eluted with Actin Elution Buffer (10mM Tris, 50mM KCl, 1mM EGTA, 1mM ATP, and 0.5mM DTT, pH 8.0). Gelsolin was eluted using Elution Buffer (defined in Gelsolin section).

Actin fractions were pooled and polymerized by 10x MEH Buffer and $MgCl_2$ to a final concentration of 1x and 2 mM, respectively. Actin was allowed to polymerize for 4 hours at room temperature. Polymerized actin was pelleted by centrifugation at 278000 x g for 20 min at 4°C. Actin pellet was resuspended and dialyzed against Buffer A for

several days. Actin was pelleted by centrifugation at 278000 x g for 15 min at 4°C to remove aggregates. Actin was gel filtered using GE Superdex S200 and stored in dialysis buffer that was exchanged every two days until needed.

For labeling, actin in Buffer A was pre-reduced with 2mM DTT for 2 hours at 4°C. Actin was buffer-exchanged into Labeling Buffer (5mM Tris, 0.1mM $CaCl_2$, 0.2mM ATP, pH 7.0) using PD-10 column. To polymerize 27μM actin, 10x KMEH was added to a final concentration of 1x. Actin was allowed to polymerize for 30 min at room temperature. 4 molar excess of maleimide-functionalized Alexa dyes was added to polymerize actin. Reaction was incubated overnight at 4°C.

Reaction was quenched with 10mM DTT. Dye aggregates were removed by centrifugation at 10000 x g for 15 min. Polymerized Actin was pelleted by centrifugation at 278000 x g for 15 min. Actin was resuspended in Buffer A. Actin was gel filtered using GE Superdex S200 to remove excess dye. Actin was stored in Buffer A and was continuously dialyzed against fresh Buffer A until needed.

Drosophila melanogaster Tropomyosins Tm1A, Tm1J, and Tm2A

Each tropomyosin was overexpressed in *E. Coli* BL-21s (DE3) expression cells. Cells were grown in Terrific Broth media containing 100 μg/mL carbenicillin until OD_{600} = 0.8. Cells were induced with 1 mM IPTG at 37°C for 4-5 hours. Cells were harvested, flash frozen, and stored at -80°C until needed. Cells were thawed and resuspended in Tm Lysis Buffer (50 mM Tris, 500 mM KCl, 5 mM BME, 1 mM PMSF, 1x Roche EDTA-free Protease Inhibitor cocktail, pH 7.5). Cells were lysed using Avestin C5 Emulsiflex and lysate was cleared by centrifugation at 167000 x g at 4°C for 1 hour. Lysate was applied to GE HisTrap excel column. Column was washed with Tm Wash Buffer (10 mM

Tris, 500 mM KCl, 5 mM BME, 10 mM Imidazole, pH 7.5). Tropomyosin was eluted with Tm Elution Buffer (10 mM Tris, 500 mM KCl, 5 mM BME, 500 mM Imidazole, pH 7.5). Cleanest fractions were pooled and then His-tagged SUMO Protease was added. Tropomyosin was dialyzed against HA Binding buffer (5 mM Potassium Phosphate, 500 mM KCl, 0.5 mM TCEP, pH 7.5)

Tropomyosin was added to GE HisTrap excel column and flow through was collected. Tropomyosin was applied to a BioRad hydroxyapatite CHT Type I cartridge. Tropomyosin was eluted with a gradient that started with 100% HA Binding Buffer and 0% HA Elution Buffer (200 mM Potassium Phosphate, 500 mM KCl, 0.5 mM TCEP, pH 7.5) and gradually increased to 0% HA Binding Buffer and 100% HA Elution Buffer. Cleanest tropomyosin fractions were pooled and was gel filtered using GE Superdex S200 column via Tm Gel Filtration Buffer (10 mM Tris, 500 mM KCl, and 0.5 mM TCEP, pH 7.5). Tropomyosin was concentrated and flash frozen in Gel Filtration Buffer + 20% Glycerol. Protein was stored at -80°C until needed.

Tropomyosins were pre-reduced with 2 mM DTT for 2 hours at 4°C. Tropomyosin was buffer-exchanged into Tm Gel Filtration Buffer without TCEP using PD-10 columns. 4 molar excess of maleimide-functionalized Alexa dyes were added to the tropomyosins. Reactions were incubated overnight at 4°C for 100% labeling. Reaction was quenched with 10 mM DTT. Dye aggregates were removed by centrifugation at 10000 x g for 15 min. Tropomyosins were gel filtered using GE Superdex S200 to remove excess dye and protein aggregates. Tropomyosins were stored in Tm Gel Filtration Buffer + 20% Glycerol until needed.

Drosophila melanogaster Tropomyosin heterodimer Tm1J/Tm2A

Tropomyosin heterodimer was overexpressed in *E. Coli* C43s (DE3) expression cells. Cells were grown in Terrific Broth media containing 100 μg/mL Carb until OD_{600} = 0.8. Cells were induced with 1 mM IPTG at 37°C for 4-5 hours. Cells were harvested, flash frozen, and stored at -80°C until needed.

Cells were thawed and resuspended in Tm Lysis Buffer. Cells were lysed using Avestin C5 Emulsiflex and lysate was cleared by centrifugation at 167000 x g at 4°C for 1 hour. Lysate was applied to GE HisTrap excel column and column was washed with Tm Wash Buffer. Tropomyosin was eluted with Tm Elution Buffer. Cleanest fractions were pooled. Tropomyosin was applied to Streptactin XT cartridge and washed with StrepTag Wash buffer (100mM Tris, 500mM KCl, 1mM EDTA, 0.5mM DTT, pH 7.5). Tropomyosin was eluted with StrepTag Wash Buffer + 50 mM Biotin. Tropomyosin fractions were pooled and concentrated. Tropomyosin was gel filtered using GE Superdex S200 column via Tm Gel Filtration Buffer. Cleanest fractions were pooled, concentrated, and dialyzed against Tm Gel Filtration Buffer + 20% Glycerol. Tm was flash frozen and stored at -80°C until needed. For labeled tropomyosins, labeling protocol mentioned in the tropomyosin section above was used.

Quantifying tropomyosins

All unlabeled and Alexa Fluor 488-labeled tropomyosins were quantified using SYPRO Ruby protein gel stain as these tropomyosins contain no endogenous tryptophans and have very few tyrosines for accurate protein quantification at UV absorbance at 280 nm.

TIRF Chamber Assembly

Preparation of Glass

Microscope slides were sonicated for 20 minutes in 3 M KOH and then rinsed with copious amounts of Milli-Q water. Slides were dried using argon or nitrogen gas. Slides were stored in a slide box at room temperature for future use. High precision coverslips were etched on one side with a diamond pen to distinguish the coverslip sides. The unetched side underwent silanization and PEGylation as described below:

Coverslips were sonicated for 20 minutes in 3M KOH and then rinsed with copious amounts of Milli-Q water. The coverslips were dried using a custom-made coverslip spinner with Teflon rotors (check Mullins lab website for parts list). The coverslips were further dried by baking at 70°C for 30 minutes. The baked coverslips were then plasma treated in a Harrick Plasma Cleaner at high power for 5 minutes. Immediately following plasma treatment, (3-Glycidloxypropyl) trimethoxysilane was sandwiched between two clean coverslips, sandwiches were placed into weighing jars, and the weighing jars were baked at 70°C for 1 hour.

Silanized coverslips were rinsed with HPLC-grade acetone to remove excess silane. 75 µL of 300 mg/mL NH_2-PEG-5000-methoxy with 3% NH_2-PEG-5000-Biotin in HPLC-grade acetone was sandwiched between two coverslips, coverslip sandwiches were placed into weighing jars, and the weighing jars were baked for 70°C for 4-5 hours. Coverslips were washed with copious amounts of Mili-Q water, dried using the coverslip spinner, and stored under vacuum at -20°C until used.

Laser cutter was used to cut three channels into 3M double-sided tape (9474LE 300LSE). These channels served as chambers for three separate experiments. To

assemble the TIRF chamber, the laser cut tape was sandwiched with a passivated coverslip and a clean microscope slide.

Total Internal Reflection Fluorescence Microscopy

Visualizing actin filaments using TIRF Microscopy was performed using a modified protocol as outlined in Hansen and Mullins (2010) and Kuhn and Pollard (2005). Briefly, TIRF chambers were blocked with 5 mg/mL K-Casein and 0.5 mg/mL B-Casein in K100MEH with TCEP (100mM KCl, 1mM $MgCl_2$, 1mM EGTA, 10mM HEPES, 0.5mM TCEP, pH 7.0). After 3 minutes, the chamber was washed with K100MEH with TCEP, removing excess blocking reagents.

To prepare the reaction mix, actin and tropomyosin (concentrations used described in figure legends) were combined with TIRF buffer with the final composition of: 200 units/mL catalase, 110 units/mL glucose oxidase, 20 mM glucose, 0.2 mM ATP, 0.2% methylcellulose cP400, 2-Mercaptoethanol, 100 mM KCl, 1 mM $MgCl_2$, 1 mM EGTA, 10 mM HEPES, pH 7.0. Reaction mix was added into the TIRF chamber and chamber was sealed using non-toxic silicone grease (Dow Corning Molykote 111).

Circular Dichroism Spectroscopy

Circular dichroism (CD) spectra acquisition and thermal denaturation was performed in a Jasco J-715 CD spectrometer using a cuvette with a 1 mm pathlength (Starna Cells, 21-Q-1). For each experiment, the cuvette was washed with Hellmanex III, followed by washing with copious amounts of ultrapure water. Cuvette was dried with argon gas.

Tropomyosin homodimers Tm1A, Tm1J, and Tm2A were prepared at a concentration of 15 μM in a buffer of 5 mM potassium phosphate, 500 mM KCl, and 5 mM DTT, pH 7.5 @ 25ºC. For each tropomyosin, spectral data was recorded between 201 nm and 280 nm, where the high-tension voltage was kept below 800 V. Melting curves were then collected at 220 nm with a resolution of 0.1 ºC during a heating rate of
1ºC/min from 25ºC to 95ºC.

References

Balasubramanian, M., Bi, E., Glotzer, M. (2004). Comparative analysis of cytokinesis in budding yeast, fission yeast and animal cells. *Current Biology*, 14(18), R806-R818.

Bronson, D., Schachat, F. (1982). Heterogeneity of contractile proteins. Differences in tropomyosin in fast, mixed, and slow skeletal muscles of the rabbit. *The Journal of biological chemistry*, 257(7), 3937-44.

Catanzariti, A., Soboleva, T., Jans, D., Board, P., Baker, R. (2004). An efficient system for high-level expression and easy purification of authentic recombinant proteins. *Protein Science*, 13(5), 1331-1339.

Dalby-Payne, J., O'Loughlin, E., Gunning, P. (2003). Polarization of Specific Tropomyosin isoforms in gastrointestinal epithelial cells and their impact on CFTR at the apical surface*. Molecular Biology of the Cell*, 14(11), 4365-4375.

D'Ambrosio, M., Vale, R. (2010). A whole genome RNAi screen of Drosophila S2 cell spreading performed using automated computational image analysis. *The Journal of Cell Biology*, 191(3), 471-478.

Gimona, M., Watakabe, A., Helfman, D. (1995). Specificity of dimer formation in tropomyosins: influence of alternatively spliced exons on homodimer and heterodimer assembly. *Proceedings of the National Academy of Sciences*, 92(21), 9776-9780.

Goins, L., Mullins, R. (2015). A novel tropomyosin isoform functions at the mitotic spindle and golgi in Drosophila*. Molecular Biology of the Cell,* 26(13), 2491-2504.

Gumbiner, B. (1996). Cell Adhesion: The molecular basis of tissue architecture and morphogenesis. *Cell,* 84(3), 345-357.

Hansen, S., Mullins, R. (2010). VASP is a processive actin polymerase that requires monomeric actin for barbed end association. *The Journal of Cell Biology*, 191(3), 571-584.

Heath, J., Dunn, G. (1978). Cell to substratum contacts of chick fibroblasts and their relation to the microfilament system. A correlated interference-reflection and high-voltage electron-microscope study. *Journal of cell science,* 29, 197-212.

Iwasa, J., Mullins, R. (2007). Spatial and temporal relationships between actin-filament nucleation, capping, and disassembly. *Current Biology*, 17(5), 395-406.

Kuhn, J., Pollard, T. (2005). Real-Time measurements of actin filament polymerization by Total Internal Reflection Fluorescence Microscopy. *Biophysical Journal,* 88(2), 1387-1402.

Mabuchi, I. (1994). Cleavage furrow: timing of emergence of contractile ring actin filaments and establishment of the contractile ring by filament bundling in sea urchin eggs. *Journal of cell science*, 107(Pt 7), 1853-62.

Monteiro, P., Lataro, R., Ferro, J., Reinach, F. (1994). Functional alpha-tropomyosin produced in E. coli. *The Journal of biological chemistry*, 269(14), 10461-6.

Percival, J., Thomas, G., Cock, T., Gardiner, E., Jeffrey, P., Lin, J., Weinberger, R., Gunning, P. (2000). Sorting of tropomyosin isoforms in synchronized NIH 3T3 fibroblasts: Evidence for distinct microfilament populations. *Cell Motility and the Cytoskeleton*, 47(3), 189-208.

Pollard, T., Cooper, J. (2009). Actin, a central player in cell shape and movement. *Science*, 326(5957), 1208-1212.

Rogers, S., Wiedemann, U., Stuurman, N., Vale, R. (2003). Molecular requirements for actin-based lamella formation in Drosophila S2 cells. *The Journal of Cell Biology*, 162(6), 1079-1088.

Sanders, C., Burtnick, L., Smillie, L. (1986). Native chicken gizzard tropomyosin is predominantly a beta gamma-heterodimer. *The Journal of biological chemistry*, 261(27), 12774-8.

Schevzov, G., Whittaker, S., Fath, T., Lin, J., Gunning, P. (2011). Tropomyosin isoforms and reagents. *BioArchitecture*, 1(4), 135-164.

Svitkina, T., Borisy, G. (1999). Arp2/3 complex and Actin Depolymerizing Factor/Cofilin in dendritic organization and treadmilling of actin filament array in lamellipodia. The Journal of Cell Biology, 145(5), 1009-1026.

Publishing Agreement

It is the policy of the University to encourage open access and broad distribution of all theses, dissertations, and manuscripts. The Graduate Division will facilitate the distribution of UCSF theses, dissertations, and manuscripts to the UCSF Library for open access and distribution. UCSF will make such theses, dissertations, and manuscripts accessible to the public and will take reasonable steps to preserve these works in perpetuity.

I hereby grant the non-exclusive, perpetual right to The Regents of the University of California to reproduce, publicly display, distribute, preserve, and publish copies of my thesis, dissertation, or manuscript in any form or media, now existing or later derived, including access online for teaching, research, and public service purposes.

DocuSigned by:
Johnny Rodriguez
42485DAAD8FB494...
Author Signature

9/4/2020
Date